HYDROGEN DIFFUSION AND TRAPPING IN A 42CrMo4 QUENCHED AND TEMPERED STEEL: INFLUENCE OF TEMPERING TEMPERATURE

A. Zafra[1], L.B. Peral and J. Belzunce

[1]Corresponding author: Alfredo Zafra García (+34 985182023) zafraalfredo@uniovi.es
University of Oviedo, Campus Universitario, East Building, 33203, Gijón, Spain

ABSTRACT

A 42CrMo4 steel quenched and tempered at different temperatures was tested via a combination of electrochemical hydrogen transient build-up permeation tests and thermal desorption analysis (TDA). The evolution of the apparent diffusion coefficient, D_{app}, versus the applied cathodic current density as microstructural hydrogen traps are progressively filled, was obtained until reaching the value of the lattice diffusion coefficient, D_L (hydrogen diffusion in the steel when all its traps are filled). TDA analyses were additionally performed to determine the binding energies related to the different microstructural traps present in the microstructures of these steel grades.

Hydrogen binding energies of 11.8, 17 and 27.4 kJ/mol were determined, these values being found not to depend on the tempering temperature. It was also demonstrated that the most energetic peak was associated with dislocations. Furthermore, both hydrogen diffusivities, D_{app} and D_L, decrease while hydrogen solubility, C_{0app}, (subsurface hydrogen concentration at the entry side when all traps are filled), and the density of hydrogen traps, N_t, increase with the hardness of the steel (hardness varies linearly with the tempering temperature in this 42CrMo4 quenched and tempered steel).

KEYWORDS: Hydrogen diffusion, hydrogen trapping, 42CrMo4, hydrogen permeation tests, TDA.

1. INTRODUCTION

Hydrogen atoms can enter into steel components during pickling, electric discharge machining, electrolytic coating from aqueous media and cathodic protection, due to corrosion phenomena in different environments, and in components submitted to contact with hydrogen-containing gases at high pressure [1–4]. Under these circumstances, hydrogen atoms can be absorbed by the steel surface and interact with the steel microstructure to produce embrittlement phenomena, characterized by a drastic reduction in the steel´s most important mechanical properties (tensile strength, elongation, fracture toughness and fatigue crack propagation rate) [5–8]. Hydrogen embrittlement takes place when the hydrogen concentration located in certain details of the steel microstructure exceeds the threshold hydrogen concentration under the applied external loads. The controlling factors of hydrogen embrittlement are stress (external and residual), the diffusible hydrogen content, the microstructure of the steel and its strength level. Therefore, the characterization of hydrogen behaviour in steels is very important in understanding, predicting, and preventing hydrogen embrittlement [9,10].

Hydrogen absorption, diffusion and segregation processes have been widely investigated to elucidate the underlying mechanisms of hydrogen embrittlement. Reliable information on hydrogen ingress from the surrounding environment into the steel, hydrogen transport inside the steel and hydrogen trapping in characteristic structural defects can be obtained using electrochemical permeation techniques, considered to be the most widespread, appropriate method for measuring hydrogen diffusivity [11–13]. Trapping site characteristics can also be determined by examining the effective diffusivity of hydrogen in the course of build-up and decay transients in hydrogen permeation experiments, but are more usually investigated using thermal desorption analysis (TDA), which monitors the rate at which hydrogen is released from a pre-charged sample submitted to continuous heating [14–18]. Strong or deep traps release their hydrogen at a higher temperature, allowing the binding energy of microstructural traps to be determined in these tests. Hydrogen traps reduce hydrogen diffusivity and increase hydrogen solubility within the steel

microstructure, consequently affecting the risk of hydrogen embrittlement and hence premature failure. In this context, hydrogen atoms are known to be retained in quenched and tempered steels (tempered martensite microstructures) in microstructural traps, such as prior austenite grain boundaries, martensitic lath and packet interfaces, dislocations, interfaces between the matrix and precipitated carbides and in interfaces between the matrix and inclusions [19–21]. These lattice imperfections explain that the hydrogen diffusion coefficient is around two orders of magnitude lower in quenched low temperature tempered steels than in pure iron [22–27].

The effect of steel hardness (or yield strength) and microstructure on hydrogen transport and trapping have been studied by many researchers. Parvathavarthini et al. [24] compared the hydrogen permeation behavior of water-quenched, air-cooled and furnace-cooled 2.25Cr1Mo steel and also investigated the effect of tempering the as-quenched structure. They found that hydrogen diffusion coefficients and solubilities are respectively inversely and directly correlated with the Vickers macrohardness of the steel. Similar results were obtained by Moli-Sanchez et al. [25] using a quenched 34CrMo4 steel tempered at different temperatures (between 200 and 680ºC). Comparable effects of hydrogen were yet obtained by Garet et al. [29] when comparing ferritic-pearlitic and bainitic CrMo steels. The same effects of tempering were also reported by Depover et al. [30] using W alloyed quenched steels, which they associated with the reduction in dislocation density produced during tempering. These authors additionally demonstrated that large carbides precipitated in the course of this treatment were not able to trap hydrogen but rather, that small carbides (with sizes below 20 nm) can act as high energy hydrogen traps. Galindo-Nava et al. [31] also demonstrated that dislocations are the main factor in controlling the mobility of hydrogen in quenched and tempered martensitic steels.

The principal aim of the present study is to contribute to a better understanding of the diffusion and trapping of hydrogen in tempered martensitic steels. A 42CrMo4 steel quenched and tempered at different temperatures (between 500ºC to 700ºC) was tested via a combination of electrochemical hydrogen transient build-up permeation tests and thermal desorption analysis (TDA). The evolution of the apparent diffusion coefficient, D_{app}, versus the applied cathodic current density was obtained until reaching the value of the lattice diffusion coefficient, D_L. The density of trapping sites, N_t, was also estimated using two different approaches. TDA analyses were additionally performed to determine the binding energies related to the different microstructural traps present in the microstructures of these steel grades.

2. EXPERIMENTAL PROCEDURE

2.1 Materials and heat treatments

A commercial 42CrMo4 steel was used in the present study. Its chemical composition is shown in Table 1.

Steel	C	Cr	Mo	Mn	Si	P	S
42CrMo4	0.42	0.98	0.22	0.62	0.18	0.008	0.002

Table 1. Chemical composition in weight% of the 42CrMo4 steel (weight %)

Hot rolled plates (250x250x12 mm^3) of 42CrMo4 were submitted to different heat-treatment sequences obtaining 5 steel grades, as specified in Table 2. In order to study the influence of the tempering temperature (i.e. the hardness level) on hydrogen diffusion and trapping, the steel was austenitized at 845ºC for 40 min, quenched in water and tempered at 700, 650, 600, 550 and 500ºC for 2 h, respectively.

Steel grade	Sequence of heat treatments
42CrMo4-700	845ºC/40min + water quenching + 700ºC/2h tempering
42CrMo4-650	845ºC/40min + water quenching + 650ºC/2h tempering
42CrMo4-600	845ºC/40min + water quenching + 600ºC/2h tempering
42CrMo4-550	845ºC/40min + water quenching + 550ºC/2h tempering
42CrMo4-500	845ºC/40min + water quenching + 500ºC/2h tempering

Table 2. Heat treatments applied to the 42CrMo4 steel

2.2 Microstructure characterization

The microstructures obtained after the application of the different heat treatments were examined under a scanning electron microscope (SEM JEOL-JSM5600) applying an acceleration voltage of 20 kV. The samples were previously ground with SiC paper until 1200 grit, polished with 6 and 1 µm diamond paste and etched with Nital-2%.

Brinell hardness measurements were performed on each sample, applying a load of 187.5 kg for 15 s using a 2.5 mm diameter spherical indenter. At least five measurements were made in all cases, subsequently calculating the average hardness value. For further information on the mechanical properties of these 42CrMo4 steel grades, the reader is referred to [32,33].

Additionally, the full width at half maximum (FWHM)) parameter was measured by means of X-ray diffraction in all the samples as an indirect estimation of the dislocation density [34,35], which is a key microstructural parameter related to hydrogen diffusion and trapping. In fact, the FWHM parameter measured on the diffraction peak is often used to assess material hardening during heat treatments [36,37]. Its value was experimentally determined using an X STRESSTECH 3000-G3R diffractometer equipped with a Cr-tube (with a wavelength, λ = 0.229 nm) on the crystallographic (211) plane of ferrite/martensite, which corresponds to a diffraction angle, 2θ, of 156.4º. The FWHM parameter is dependent not only on the dislocation density, but is also influenced by structural distortion, thus constituting suitable parameter indirectly related to hydrogen diffusion and trapping.

2.3 Determination of trap binding energies

Thermal desorption analysis (TDA) was used to describe the traps present in these steel grades. Hydrogen pre-charged samples were heated under a defined temperature profile, so the stored hydrogen atoms effuse differently depending on the kind of trapping site and its associated activation energy. The trap activation energy, E_a, was thus determined by detecting the released hydrogen as a function of the heating rate [38,39]. The trap biding energy, E_b, was then calculated, assuming $E_a=E_b+E_L$ (E_L being the activation energy of hydrogen diffusion in an iron lattice, which has a value of 8 kJ/mol [40]).

Assuming that the egress of hydrogen from a trap site is a thermally activated process, the hydrogen evolution rate from trapping sites can be written according to the following expression (Equation 6).

$$\frac{dX_H}{dt} = A(1 - X_H) \cdot e^{\left(-E_a/_{RT}\right)} \qquad (6)$$

where X_H is the fraction of hydrogen evolved from a trapping site characterized by an activation energy E_a, and A is a constant.

Hence, when a hydrogen-charged specimen is heated at a uniform rate, $\phi(dT/dt)$, a hydrogen peak related to the trap activation energy is detected at a certain temperature, T_p. Using the model developed by Lee and Lee [41], derived from Fick's second law, the trap activation energy, E_a, can be calculated from the slope of the linear regression obtained when plotting $\ln(\phi/T_p^2)$ versus $1/T_p$, according to Equation 7. This equation is valid for low trap occupancy in the case of low lattice hydrogen contents [16,38].

$$\frac{\partial\left[ln\left(\phi/T_p^2\right)\right]}{\partial\left(1/T_p\right)} = -\frac{E_a}{R} \quad (7)$$

These tests were performed on a LECO DH603 hydrogen analyzer, using the following heating rates: 4800, 3600, 2400, 1800, 1200, 800 and 400ºC/h.

To evaluate the activation trap energies of each steel grade, small cylindrical samples with a diameter of 10 mm and a length of 30 mm (≈20g weight) were thermally pre-charged with gaseous hydrogen in a high-pressure reactor at 19.5 MPa and 450ºC for 21 h. Operating in this way, all the 42CrMo4 samples were saturated with hydrogen by the end of the charging phase. However, during the required cooling phase to be able to safely remove the specimens from the reactor, significant hydrogen losses took place despite maintaining the hydrogen pressure. All the charged specimens were subsequently removed from the reactor and rapidly immersed in liquid nitrogen (-196ºC), where they were kept until the moment of testing, once again in order to limit hydrogen losses. Before each measurement, the pin was cleaned with acetone and carefully dried using cold air. Hydrogen contents between 1.2 and 1.9 ppm were finally measured in the different samples in a LECO DH603 analyzer.

2.4 Hydrogen permeation experiments

The hydrogen transport and trapping behaviour of 42CrMo4 steel quenched and tempered at different temperatures (700, 650, 600, 550 and 500ºC for 2 h) was characterized by means of electrochemical permeation tests. Flat specimens measuring 20x20 mm, with a thickness of between 0.7 and 1 mm depending on the steel grade, were used in this study (with a circular exposed area of 1.25 cm^2). As the surface condition of the specimen is very important to obtain reliable results in these tests [42–44], both sides were ground with SiC paper until 1200 grit, then polished with 6 µm diamond paste and cleaned with acetone prior to testing.

The permeation tests were performed in a double electrolytic cell based on the one developed by Devanathan and Stachurski [45], as is shown schematically in Figure 1(a). With an approximate volume of 300 ml, both cells satisfy the ASTM G148 [46] recommendation of a solution volume-to-surface area ratio greater than 20 ml/cm^2.

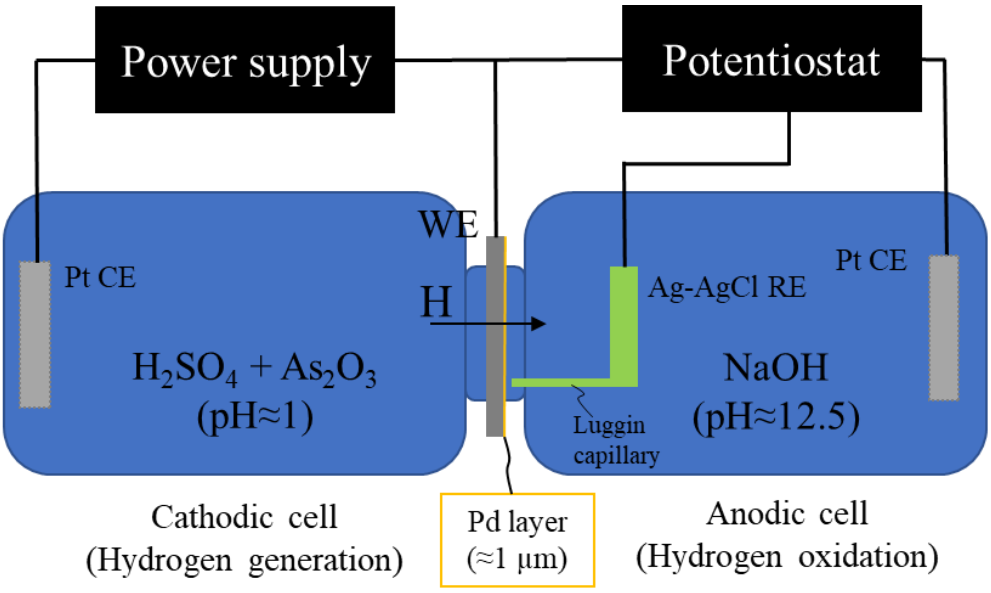

(a)

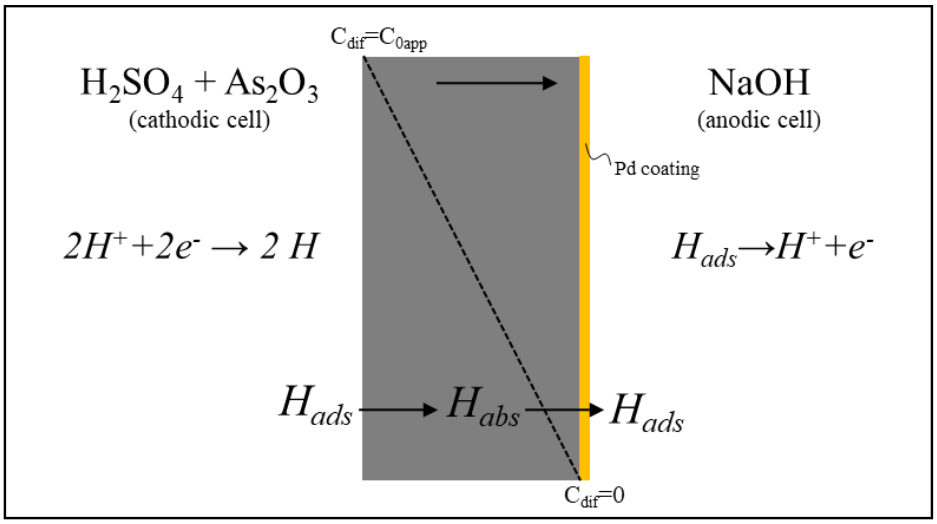

(b)

Figure 1 (a) Scheme of the modified D-S double-cell employed in the hydrogen permeation experiments; (b) hydrogen reduction and oxidation reactions.

Both cells are separated by the steel specimen, which represents the working electrode (WE) in each cell. The cathodic cell, where hydrogen generation takes places (applying a cathodic current, hydrogen is cathodically generated and hydrogen atoms are adsorbed on the surface of the metal), was filled with an acid solution (pH≈1) composed of 1M H_2SO_4 and 0.25 g/l As_2O_3 to mitigate hydrogen recombination reactions [28,47–49]. The anodic cell, on the other side of the specimen and where hydrogen oxidation occurs, was filled with a basic solution (pH≈12.5) of 0.1M NaOH. The hydrogen reduction and oxidation reactions that take place in each cell are shown in Figure 1(b). Thin platinum plates with a total surface area of 1 cm^2 (similar to the specimen's permeated area) were used as counter electrodes (CE). A reference silver/silver chloride electrode (Ag/AgCl, RE) with a Luggin capillary was employed in the anodic cell and the equipment used for data acquisition was a pocketSTAT Ivium potentiostat with a current operation range of ±10 mA. All tests were performed at room temperature.

Before commencing the tests, the background current density in the anodic cell must be reduced to a steady-state value below 0.1 $\mu A/cm^2$ and was subtracted from the measured oxidation current prior to data analysis. Hydrogen oxidation was enhanced in the anodic cell, ensuring a virtually zero hydrogen concentration on the exit side of the specimen (Figure 1(b)) via the application of a palladium coating. This coating, with a thickness of around 1-2 µm, measured under the SEM, was electrodeposited on the anodic side of the sample from a bath of commercial palladium containing 2 g/l of Pd, applying a current density of 3 mA/cm^2 for 5 min. In fact, there is general consensus as to the importance of using palladium coatings on the detection side of ferrous samples so that the permeation results may be reliably exploited in order to ensure the oxidation of hydrogen atoms on palladium-coated surfaces under most charging conditions [50]. Moreover, the possibility of having introduced hydrogen in the sample during the process of Pd electrodeposition was discarded, as different hydrogen measurements were performed on the Pd-coated samples obtaining values below 0.1 ppm in all cases.

Consequently, the permeation method employed in this study, shown in Figure 2, consisted in recording several partial build-up permeation transients by sequentially increasing the cathodic current density until reaching a steady-state value of the hydrogen diffusion coefficient. Operating in this way, saturation of all the microstructural traps is ensured in the last transients, thus allowing the true value of the lattice hydrogen diffusion coefficient of the steel, D_L (hydrogen diffusion barely affected by the presence of microstructural traps), to be obtained [15,51–53].

Depending on the hydrogen trapping capacity of each steel grade, different stepped permeation tests were performed, usually increasing the cathodic current in 0.5 or 1 mA/cm^2 steps until reaching saturation, i.e. a constant value of the diffusion coefficient. Nonetheless, the first permeation transient for all the steel grades was always obtained under a cathodic current of 0.5 mA/cm^2 in order to evaluate the diffusivity of each steel grade under the condition of low hydrogen trap occupancy. Table 3 shows all the stepped build-up permeation tests performed on the different steel grades.

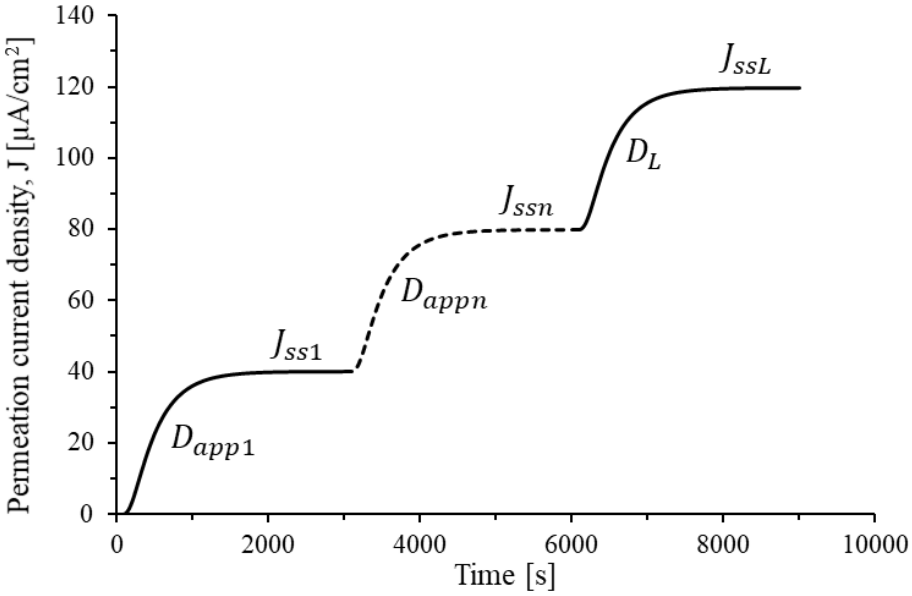

Figure 2. Hydrogen stepped build-up permeation transients applied in this study

Steel Grade	J_c [mA/cm^2]
42CrMo4-700	0.25+0.25+0.5+1
	0.5+0.5
	0.5+0.5+0.5+0.5+0.5+0.5+0.5+0.5
	0.5+0.5+1
	0.5+0.5+1+1+1
	0.25 (2 tests)
	0.5 (2 tests)
	0.75
	0.8
42CrMo4-650	0.5+0.5+0.5+0.5+0.5+0.5+0.5+0.5
	0.5+0.5+1
	0.5+0.5+1+1+1
42CrMo4-600	0.5+0.5+0.5+0.5+0.5
	0.5+0.5+0.5+0.5
	0.5+0.5+1
	0.5+0.5+1+1+1+1
	0.5+0.5+1+1+1+1+1
	0.5
	0.8
42CrMo4-550	0.5+0.5+0.5+0.5+0.5
	0.5+0.5+1
	0.5+0.5+1+1+1+1+1
	0.5+0.5+1+1+1+1+1+1 (2 tests)

42CrMo4-500	0.5+0.5
	0.5+0.5+1
	0.5+0.5+1+1+1+1 (2 tests)
	0.5+0.5+1+1+1+1+1+1+1 (2 tests)
	0.8

Table 3. Stepped build-up permeation transients performed on each steel grade

As for data analysis, the apparent hydrogen diffusion coefficient, D_{app}, was calculated in each permeation transient according to the "time lag (t_{lag})" method, using Equation (1), derived from Fick's solutions under the appropriate boundary conditions [46].

$$D_{app} = \frac{L^2}{M \cdot t_{lag}} \quad (1)$$

L being the specimen thickness; t_{lag}, the time needed to reach 63% of the steady-state permeation current, J_{ss}; and *M*, a constant with a value equal to 6 (for $J=63\%J_{ss}$).

The apparent sub-surface hydrogen concentration on the charging side of the sample, C_{0app}, can be determined according to Equation (2):

$$C_{0app} = \frac{J_{ss} \cdot L}{D_{app} \cdot F} \quad (2)$$

where J_{ss} is the steady-state permeation current density and *F*, the Faraday constant (96485 C/mol). C_{0app} can be converted from mol/cm^3 to ppm wt. by multiplying by M_H/ρ_{Fe}, M_H being the molar mass of hydrogen (1 g/mol) and ρ_{Fe} the density of iron (7.87 g/cm^3). It is worth to mention here that the hydrogen subsurface concentration, C_{0app}, depends on the sample thickness when permeation tests are done using thin membranes, being on the contrary independent on thickness in the case of thick membranes [54,55].

Stepped build-up hydrogen permeation transients were also used to evaluate the density of hydrogen traps, N_t. The mathematical formulation that allows the calculation of N_t is based on the formalisms developed by McNabb-Foster [56] and Oriani [22], subsequently improved by Kumnick and Johnson [57,58], who proposed two different approaches for determining the value of N_t depending on the degree of trap occupancy.

When trap occupancy is low, i.e the first permeation transient, the density of trapping sites, N_t, can be determined according to Equation (3),

$$N_t = N_L \left(\frac{D_L}{D_{app}} - 1 \right) \cdot exp\left(-\frac{E_b}{R \cdot T} \right) \quad (3)$$

where D_L is the value of the lattice hydrogen diffusion coefficient of the studied steel (obtained in the last transient, when all traps are filled); $D_{app,}$ the apparent hydrogen diffusion coefficient calculated in the first permeation transient to guarantee low trap occupancy; E_b, the trap binding energy, estimated from TDA measurements in this study; R, the gas constant; and T, the absolute temperature (298 K). N_L is the density of the interstitial sites in the steel, which can be calculated as proposed by Krom and Bakker [59] by means of Equation (4).

$$N_L = \frac{N_A \cdot \beta \cdot \rho_{Fe}}{M_{Fe}} \quad (4)$$

N_A being the Avogadro constant (6.022 10^{23} at/mol); β=6, the number of tetrahedral interstitial sites per atom in the Fe BCC crystal lattice; M_{Fe}, the molar mass of iron (55.8 g/mol); and ρ_{Fe}, the density of iron (7.87 g/cm^3). The value of N_L obtained using Equation (6) is 5.1□10^{29} sites/m^3.

For high trap occupancy (trap saturation), the trapping site density, N_t, is calculated by means of Equation (5):

$$N_t = \frac{C_{0app}}{3}\left(\frac{D_{LFe}}{D_L} - 1\right) \cdot N_A \qquad (5)$$

where C_{0app} is the apparent hydrogen sub-surface concentration on the charging side of the sample, calculated from Equation (2) in the last build-up transient; D_L is the lattice hydrogen diffusion coefficient estimated in this last build-up transient, where traps are fully filled; D_{LFe} is the value of the lattice hydrogen diffusion coefficient in pure iron (a value of 7.3□10^{-9} m^2/s, as reported by Kiuchi et al. [23], was considered in this paper); and N_A is the Avogadro constant. The same approach was used by Yen and Huang [60], Dong et al. [61] and Izadi et al. [62], among others.

3. RESULTS

3.1 Microstructure characterization

The SEM microstructures of the 5 grades of 42CrMo steel are shown in Figure 3 under a magnification of 10000x. The results of Brinell hardness, HB, and the FWHM parameter measured on each grade are given in Table 4 and plotted in Figure 4 versus the tempering temperature.

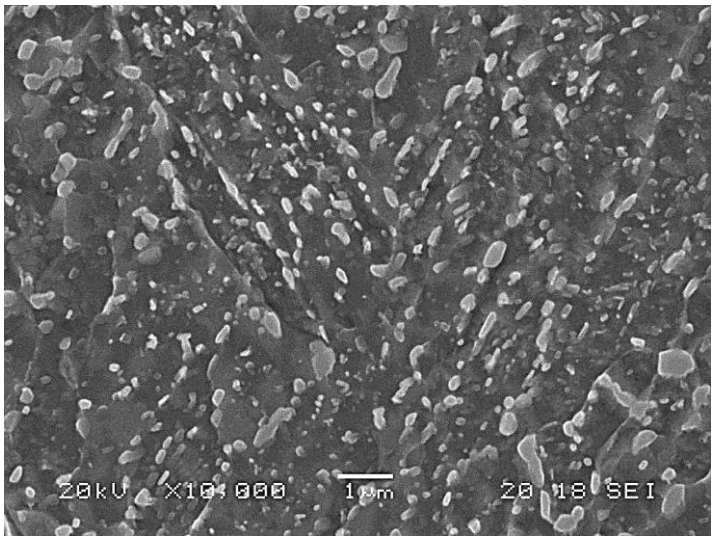

(a)

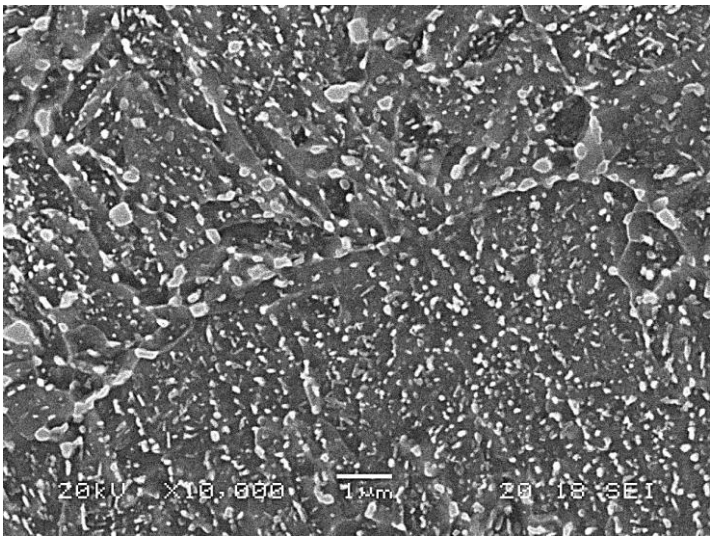

(b)

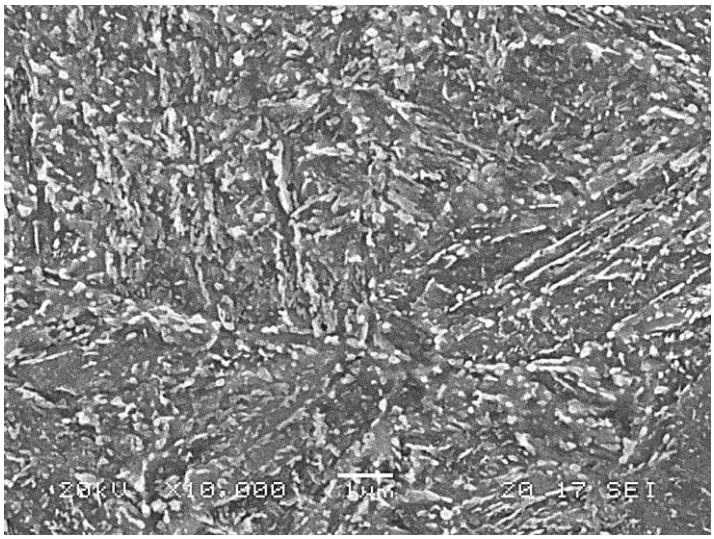

(c)

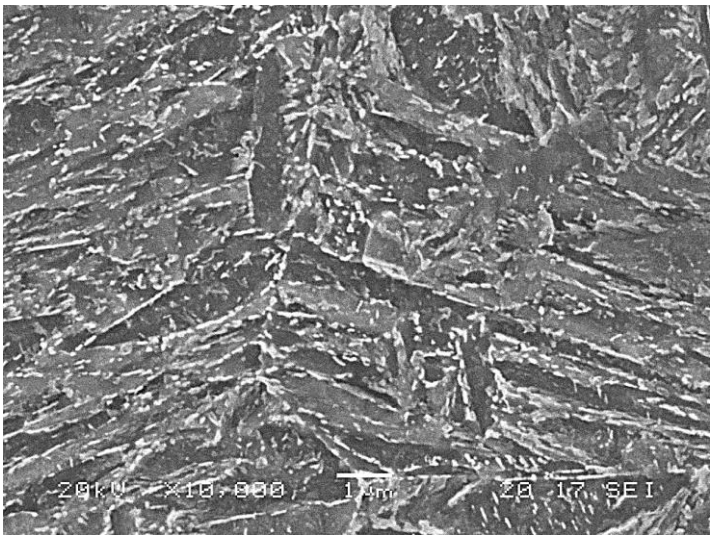

(d)

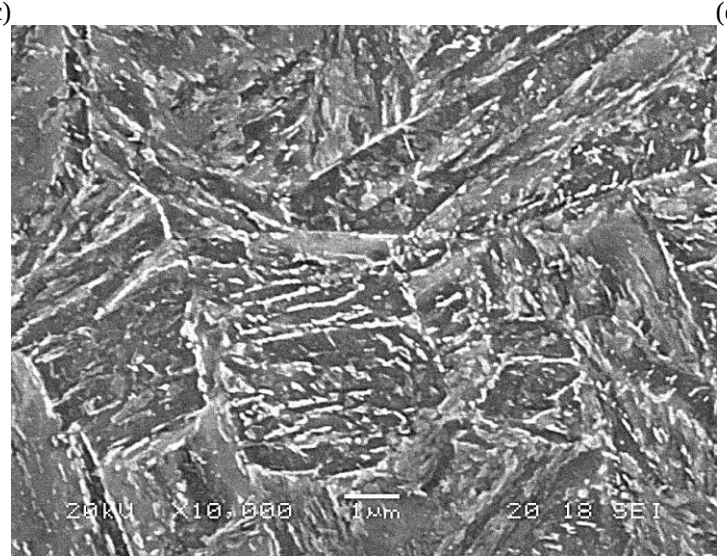

(e)

Figure 3. SEM microstructures of 42CrMo4 steel quenched and tempered (2h) at (a) 700ºC, (b) 650C, (c) 600ºC (d) 550ºC, and (e) 500ºC (10.000x)

The microstructure of all these 42CrMo4 steel grades was tempered martensite. It is observed that as the tempering temperature increases, the acicularity of the microstructure decreases, as does the distortion of the crystalline structure. Carbide precipitation also increases with tempering temperature. Elongated carbides precipitated along grain and martensitic lath/packet/block boundaries at low tempering temperatures (500 and 550ºC), then break up, globulize, and finally grow to yield a more uniform distribution as the tempering temperature increases. This carbide growth is very clearly seen when comparing microstructures of the steel tempered at 600, 650 and 700ºC.

Furthermore, it is well known that, as the tempering temperature increases, more internal residual stresses are released, the dislocation density is reduced and thus hardness and the diffraction peak width (FWHM) likewise decrease [36,63–65]. This fact is reflected in Figure 4, which shows the excellent linear correlation between the tempering temperature with the Brinell HB hardness (R^2=0.98), and the FWHM parameter (R^2=0.97). As previously stated, the latter is a parameter frequently used as an indicator of the microstructural hardening that alloys submitted to surface treatments undergo and can thus be used as an indirect measure of the dislocation density and the corresponding internal stresses [36,37,63–65]. It may be here recalled that in quenched and tempered steel microstructures, dislocations re-arranged in cells and these cell interfaces also correspond to lath, packet and block martensite interfaces, where most of carbides

also precipitate, being very difficult to separate the contribution as hydrogen traps of all these different microstructural features.

Steel grade	Heat treatment	HB	FWHM [º]
42CrMo4-700	845ºC/40min + WQ + 700ºC/2h	201	1.79
42CrMo4-650	845ºC/40min + WQ + 650ºC/2h	246	1.93
42CrMo4-600	845ºC/40min + WQ + 600ºC/2h	281	2.00
42CrMo4-550	845ºC/40min + WQ + 550ºC/2h	307	2.23
42CrMo4-500	845ºC/40min + WQ + 500ºC/2h	335	2.41

Table 4. Heat treatments, hardness and FWHM of the different 42CrMo4 steel grades

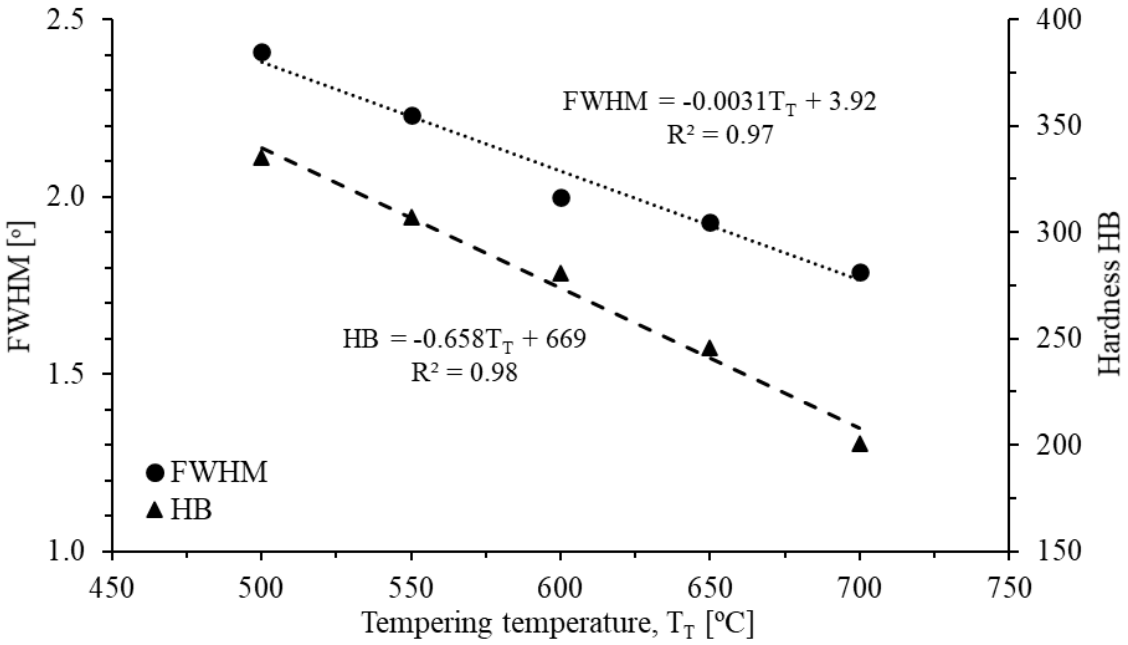

Figure 4. Evolution of FWHM and HB in terms of the applied tempering temperature

3.2 Determination of trap binding energies

Figure 5 shows an example of hydrogen evolution during the thermal desorption analysis (TDA) performed on the 42CrMo4 steel tempered at 700ºC under three different heating rates: 1800, 1200 and 800ºC/h. Three desorption peaks, associated with three different hydrogen traps, are clearly detected in all cases, shifting to higher temperatures as the heating rate increases. It is worth noting that the second and third peaks were much more intense than the first one, meaning that a greater volume of hydrogen is trapped in their corresponding traps.

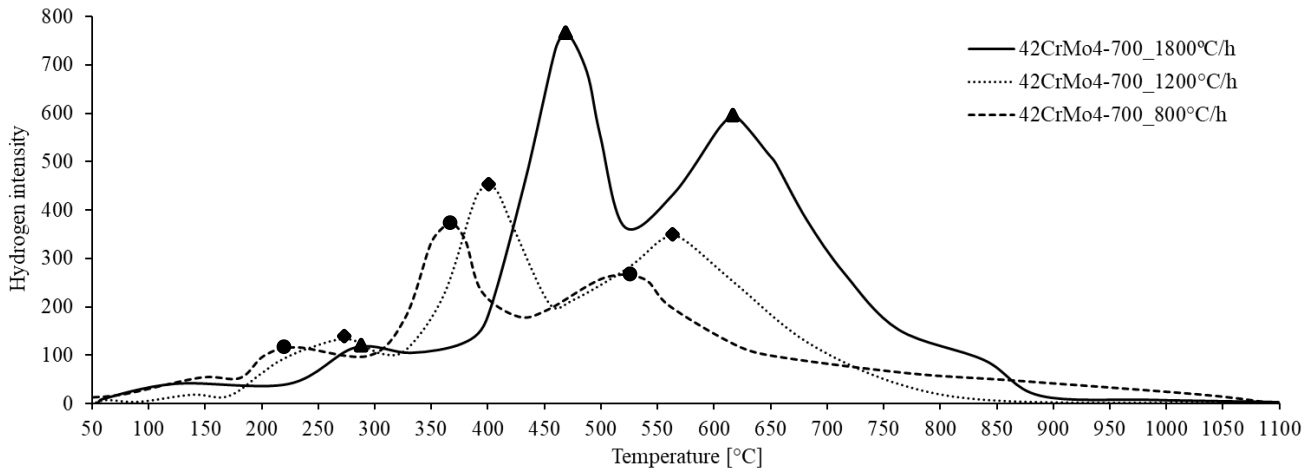

Figure 5. Thermal desorption analysis of the 42CrMo4-700 grade under three different heating rates

Considering now all the applied heating rates, Figure 6 shows the linear regression obtained between $\ln(\phi/T_p^2)$ and (1/Tp), for the same steel tempered at 700ºC. Excellent regressions (R^2 above 0.95) were obtained for the three peaks, corresponding respectively to activation energies, E_a, of 21, 25 and 35 kJ/mol.

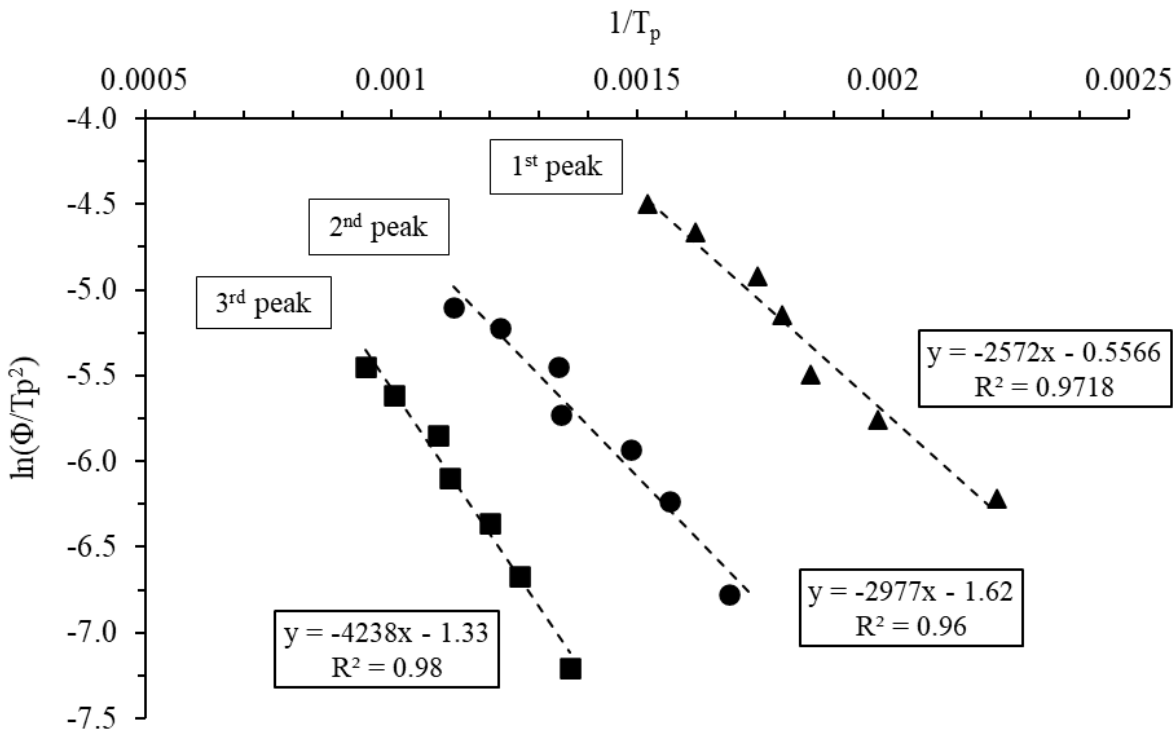

Figure 6. Linear regressions for the determination of trap activation energies, 42CrMo4-700.

Thermal desorption analysis was also applied to the other 42CrMo4 steel grades. In fact, Figure 7 compares the desorption profiles of the 42CrMo4 steel grades tempered at 700, 650, 600, 500 and 500ºC, under the same heating rate of 2400ºC/h.

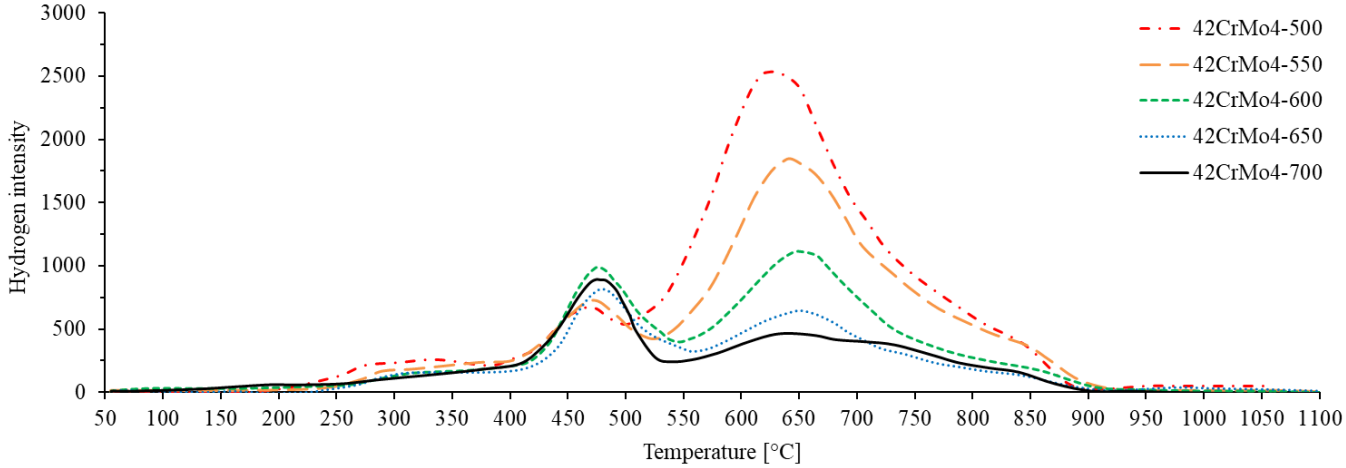

Figure 7. Thermal desorption analysis of 42CrMo4 steel quenched and tempered at 500, 550, 600, 650 and 700ºC under a heating rate of 2400ºC/h

Three peaks were also identified in all these grades. Note that the intensities of the first and second peaks were quite similar for the five tempering temperatures, while the intensity of the third peak increases considerably when the tempering temperature decreases.

Table 5 shows the slope, m, of the $\ln(\phi/T_p^2)$ versus (1/Tp) plots, the R^2 determination coefficient and the activation energy, E_a, calculated from the TDA analysis performed on all the 42CrMo4 steel grades. The excellent regressions obtained in all these analyses are also worth noting, with determination coefficients, R^2, above 0.9 in all cases.

Steel Grade	1st Peak			2nd Peak			3rd Peak		
	E_a [kJ/mol]	m	R^2	E_a [kJ/mol]	m	R^2	E_a [kJ/mol]	m	R^2
42CrMo4-700	21.4	-2572	0.97	24.8	-2977	0.96	35.2	-4238	0.98
42CrMo4-650	19.9	-2391	0.90	26.0	-3125	0.98	35.1	-4222	1.00
42CrMo4-600	17.7	-2133	0.97	24.0	-2886	0.98	35.5	-4265	0.99
42CrMo4-550	19.3	-2324	0.93	25.2	-3033	0.97	35.6	-4286	0.98
42CrMo4-500	20.1	-2413	0.94	25.1	-3016	0.98	35.7	-4288	0.97

Table 5. Trap activation energies, E_a, and determination coefficient, R^2, associated with the three desorption peaks determined in all the 42CrMo4 steel grades

However, the trap binding energy, E_b, (instead of E_a) is the trapping parameter usually reported in literature (it is also the parameter used in Equation (4)). Therefore, Table 6 shows the trap binding energies, E_b, determined for each steel grade.

Steel Grade	1st Peak	2nd Peak	3rd Peak
	E_b [kJ/mol]	E_b [kJ/mol]	E_b [kJ/mol]
42CrMo4-700	13.4	16.8	27.2
42CrMo4-650	11.9	18.0	27.1
42CrMo4-600	10.2	16.0	27.5
42CrMo4-550	11.3	17.2	27.6
42CrMo4-500	12.1	17.1	27.7
Average	11.8±1.2	17.0±0.7	27.4±0.2

Table 6. Trap binding energies, E_b, determined in 42CrMo4 steel grades ($E_b=E_a-E_L$)

According to the results shown in Table 6, the binding energy associated with each desorption peak is practically the same in all the steel grades, regardless of the tempering temperature, a finding in line with the results reported by Wei and Tsuzaki [66]. Consequently, three different hydrogen traps with average binding energies of 11.8, 17.0 and 27.4 kJ/mol were identified in the 42CrMo4 steel quenched and tempered at 500-700ºC.

Assuming that most vacancies are removed in the course of tempering [67], the first peak, with a binding energy of 11.8 kJ/mol, may be associated with interfaces between the alloyed carbides $(Fe, Cr, Mo)_3C$ and the ferritic matrix [68,69], and the second peak, with a binding energy of 17.0 kJ/mol, to hydrogen trapped in lath, block and packet martensite interphases [20,70,71]. The third peak, with a binding energy of 27.4 kJ/mol is identified with dislocations [20,41,70]. A significant, continuous increase in the intensity of this peak with decreasing tempering temperature can be observed in Figure 7, reflecting the well-known fact that dislocation density strongly increases with decreasing tempering temperature. In fact, many authors [66,72] have considered that dislocations are the governing trap site responsible for hydrogen trapping in quenched and tempered Cr-Mo steels, and trapping energies in the range of 26-30 kJ/mol are usually assumed for dislocations in steels [15,40,41,61,73–80]. The E_b value of 27 kJ/mol calculated in this study is in line with all these previous studies.

Furthermore, in order to confirm that the aforementioned third peak corresponds to hydrogen trapped in dislocations, two additional TDA analyses were performed:

- First, several 42CrMo4-500 hydrogen pre-charged samples were exposed to air at room temperature (RT) for 400 h (17 days) in order to release the reversible trapped hydrogen. TDA analysis at 1200ºC/h of these samples, shown in Figure 8, revealed that the first and second desorption peaks virtually disappeared (weakly trapped hydrogen). Moreover, the activation energy associated with the third peak increased to 39.8 kJ/mol (E_b=31.8 kJ/mol). This slight increase in binding energy may be due to the RT release of hydrogen trapped in the weakest locations within dislocations [20].

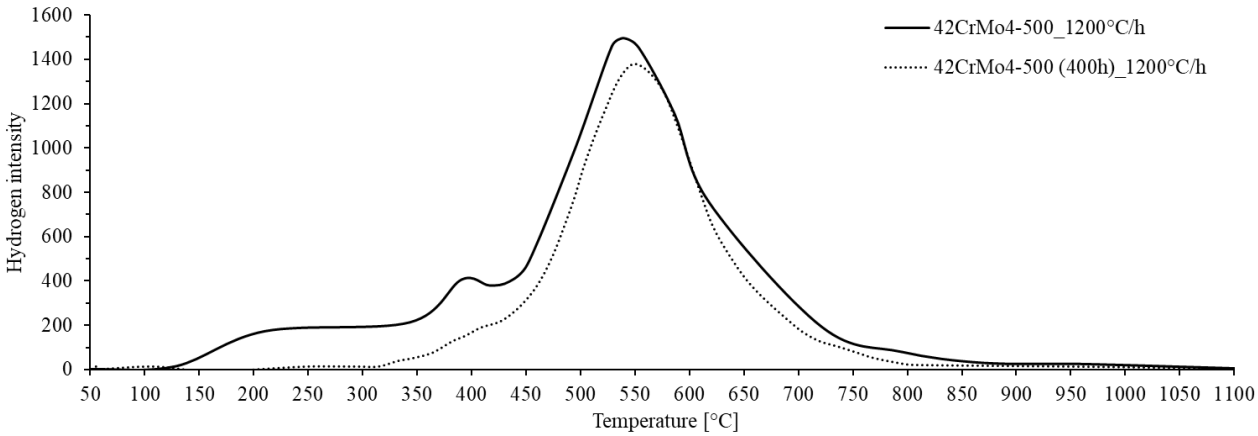

Figure 8. Thermal desorption analysis of 42CrMo4-500 and 42CrMo4-500 after 400h of air exposure under a heating rate of 1200ºC/h

- A similar TDA analysis was subsequently performed on samples of the 42CrMo4-700 steel which had been previously submitted to a small tensile plastic deformation of 0.5%. The results are shown in Figure 9, which compares the TDAs of the un-deformed and the plastically strained samples under the same heating rate, 1200ºC/h. In both cases, a small first peak and two successive larger peaks were detected, the third peak being more intense for the strained sample, where a binding energy value of 29.8 kJ/mol was calculated, slightly higher than that of the undeformed sample (27.4 kJ/mol). It is well known that the main effect induced by plastic deformation is dislocation multiplication (increase in dislocation density) [57,70,81,82]; hence the third peak may undoubtedly be related to dislocations.

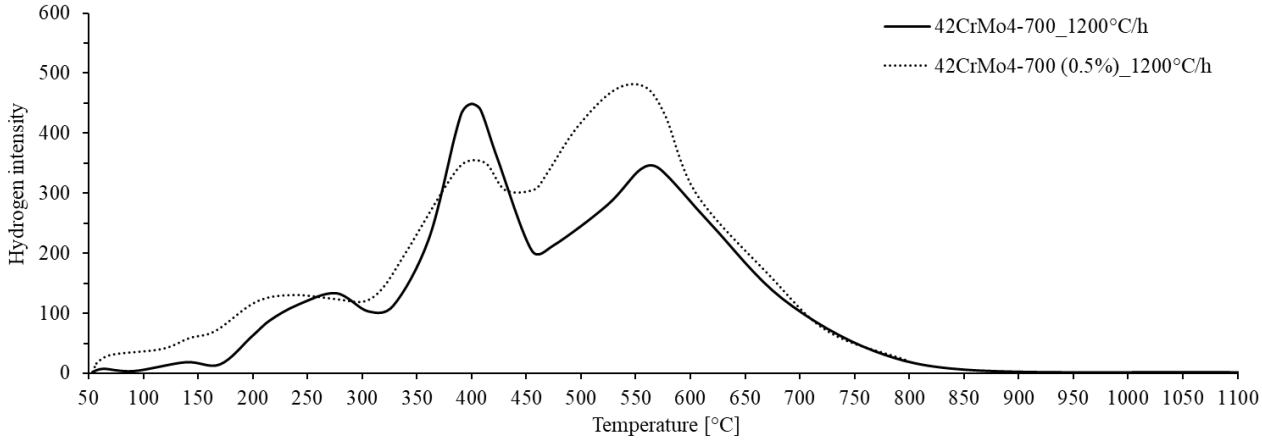

Figure 9. Thermal desorption analysis of undeformed and 0.5% strained samples of 42CrMo4 steel quenched and tempered at 700ºC under a heating rate of 1200ºC/h

3.3 Stepped build-up permeation tests

Figure 10 shows the results of some of the stepped build-up permeation tests performed on the studied steel grades. The evolution of the permeation current, J, in the successive permeation build-up transients obtained when the cathodic current density, J_c, was incrementally increased can be observed in this figure. Tests with different cathodic current density increases are plotted in Figure 10 according to the steel grade: for the softer grades, tempered at 700ºC and 650ºC, the tests consisted of 0.5 mA/cm^2 increases until reaching a final cathodic current density of 4 mA/cm^2; while for the medium-to-high hardness steel grades, tempered at 600, 550 and 500ºC, the current increases were 0.5+0.5+1+…+1 mA/cm^2, until reaching 6, 7 and 8 mA/cm^2, respectively.

Note that it is difficult to compare the permeation behaviour between steel grades from the curves shown in Figure 10, mainly due to the effect of the sample thickness (different sample thicknesses were tested, between 0.7 and 1 mm) and the influence of the charging cathodic current density.

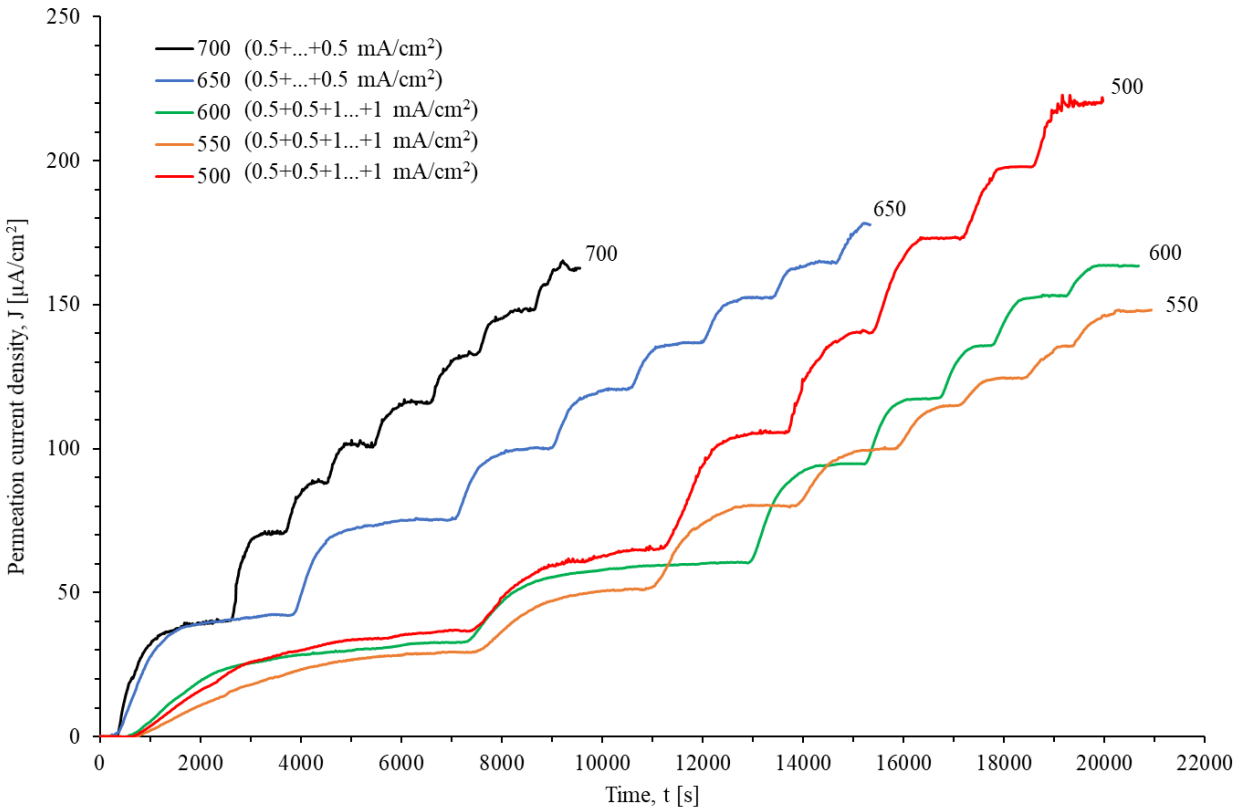

Figure 10. Permeation current density measured on the hydrogen stepped build-up transients performed on the 42CrMo4 steel grades.

In order to compare the permeation behaviour of all the studied steel grades, the normalized permeation transients corresponding to an initial cathodic current density of 0.5 mA/cm^2 (empty traps) and to the final applied cathodic current density when most hydrogen traps were fully filled are shown in Figures 11(a) and (b) respectively. In order to remove the dependence of the experimental data on the applied cathodic current density and sample thickness, test results were represented using J/J_{ss} vs. t/L^2 coordinates. Thus, the permeation current density was divided by the steady-state permeation current density reached at the end of the respective permeation transient (dimensionless parameter) and time was divided by the square of the sample thickness.

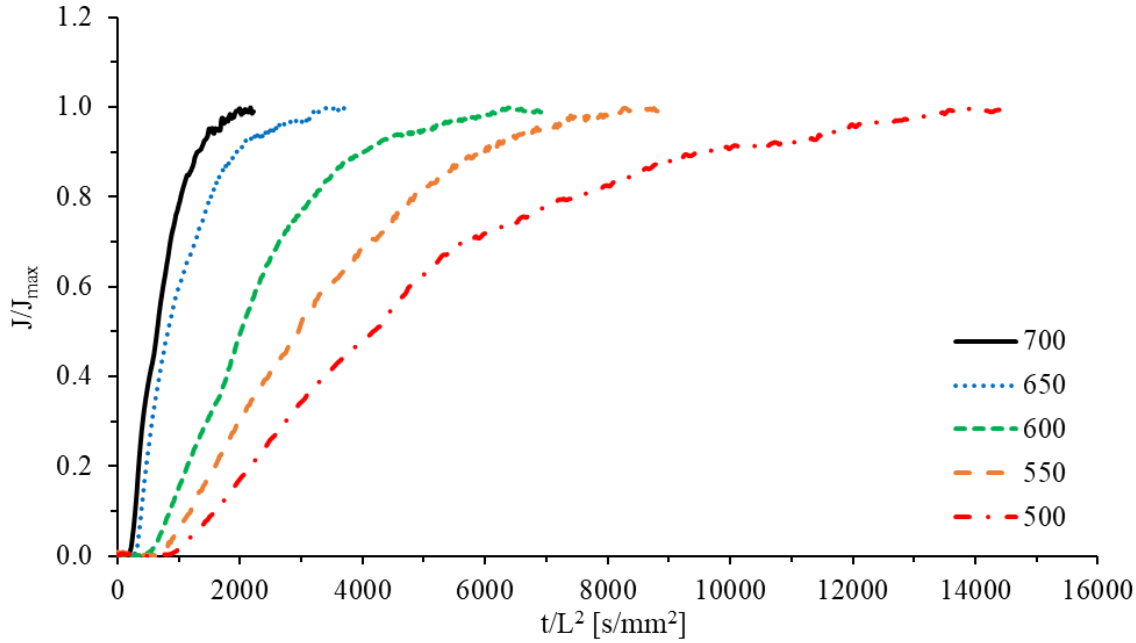

(a)

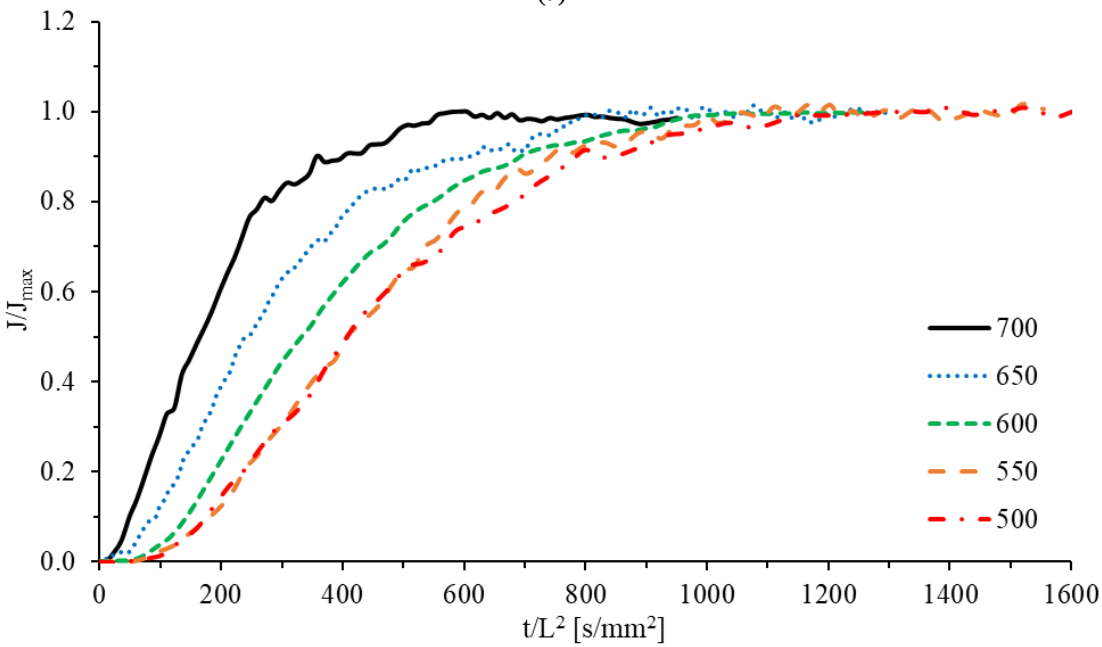

(b)

Figure 11. Normalized permeation curves of (a) the first (0.5 mA/cm^2, empty traps) and (b) the last (traps fully filled) permeation transients in all the 42CrMo4 steel grades.

Regarding Figure 11(a), it can be clearly observed that hydrogen permeation flux (hydrogen transport) is progressively delayed as the tempering temperature of the steel decreases (increase in dislocation density, hydrogen traps and hardness). As regards the situation when most hydrogen traps are filled, however, the permeation curves shown in Figure 11(b) reveal that the dependence of the hydrogen permeation flux on the tempering temperature is now weaker. When most hydrogen traps are filled, the effect of hydrogen traps on hydrogen transport is minimized.

The permeation parameters t_{lag}, D_{app}, % saturation (based on D_{app}), and C_{0app} calculated on all these transients are jointly presented in Table 7.

Steel Grade	Thickness, L [mm]	Permeation transient	J_c [mA/cm^2]	J_{ss} [μA/cm^2]	t_{lag} [s]	D_{app} [m^2/s]	Saturation [%]	C_{0app} [ppm]
42CrMo4-700	0.95	1	0.5	50	555	$2.7\square10^{-10}$	36	---
		2	1.0	89	260	$5.8\square10^{-10}$	77	---
		3	1.5	111	220	$6.8\square10^{-10}$	91	---
		4	2.0	127	200	$7.5\square10^{-10}$	100	1.7
		5	2.5	144	215	$7.0\square10^{-10}$	93	2.1
		6	3.0	165	210	$7.2\square10^{-10}$	95	2.3
		7	3.5	185	190	$7.9\square10^{-10}$	105	2.3
		8	4.0	202	200	$7.5\square10^{-10}$	100	2.7
42CrMo4-650	1.02	1	0.5	42	844	$2.1\square10^{-10}$	37	---
		2	1.0	75	542	$3.2\square10^{-10}$	58	---
		3	1.5	100	448	$3.9\square10^{-10}$	71	---
		4	2.0	121	384	$4.5\square10^{-10}$	82	---
		5	2.5	137	336	$5.2\square10^{-10}$	94	3.6
		6	3.0	152	316	$5.5\square10^{-10}$	100	3.7
		7	3.5	165	315	$5.5\square10^{-10}$	100	4.0
		8	4	178	336	$5.2\square10^{-10}$	94	4.6
42CrMo4-600	0.96	1	0.5	33	1992	$7.7\square10^{-11}$	17	---
		2	1	63	1056	$1.5\square10^{-10}$	32	---
		3	2	98	594	$2.6\square10^{-10}$	57	---
		4	3	121	408	$3.8\square10^{-10}$	82	---
		5	4	140	348	$4.4\square10^{-10}$	97	4.0
		6	5	158	360	$4.3\square10^{-10}$	93	4.7
		7	6	169	336	$4.6\square10^{-10}$	100	4.7
42CrMo4-550	0.90	1	0.5	30	2955	$4.6\square10^{-11}$	13	---
		2	1	51	1192	$1.1\square10^{-10}$	33	---
		3	2	80	870	$1.6\square10^{-10}$	46	---
		4	3	100	638	$2.1\square10^{-10}$	62	---
		5	4	115	480	$2.8\square10^{-10}$	83	---
		6	5	125	398	$3.4\square10^{-10}$	100	4.4
		7	6	136	510	$3.2\square10^{-10}$	100	5.1
		8	7	148	405	$3.3\square10^{-10}$	100	5.3
42CrMo4-500	0.70	1	0.5	37	2430	$3.4\square10^{-11}$	9	---
		2	1	65	1155	$7.1\square10^{-11}$	18	---
		3	2	106	763	$1.1\square10^{-10}$	27	---
		4	3	141	540	$1.5\square10^{-10}$	39	---
		5	4	173	480	$1.7\square10^{-10}$	43	---
		6	5	198	360	$2.3\square10^{-10}$	58	---
		7	6	220	225	$3.6\square10^{-10}$	93	5.6
		8	7	240	215	$3.8\square10^{-10}$	98	5.8
		9	8	255	210	$3.9\square10^{-10}$	100	6.0

Table 7. Results obtained from the permeation curves shown in Figure 10 for the different 42CrMo4 grades

Moreover, the entire set of data corresponding to all the experimental build-up permeation tests carried out under the different cathodic current density transients for all the 42CrMo4 steel grades (see Table 3) is shown in Figure 12, where the evolution of the apparent hydrogen diffusion coefficient, D_{app}, is represented versus the applied cathodic current density, J_c.

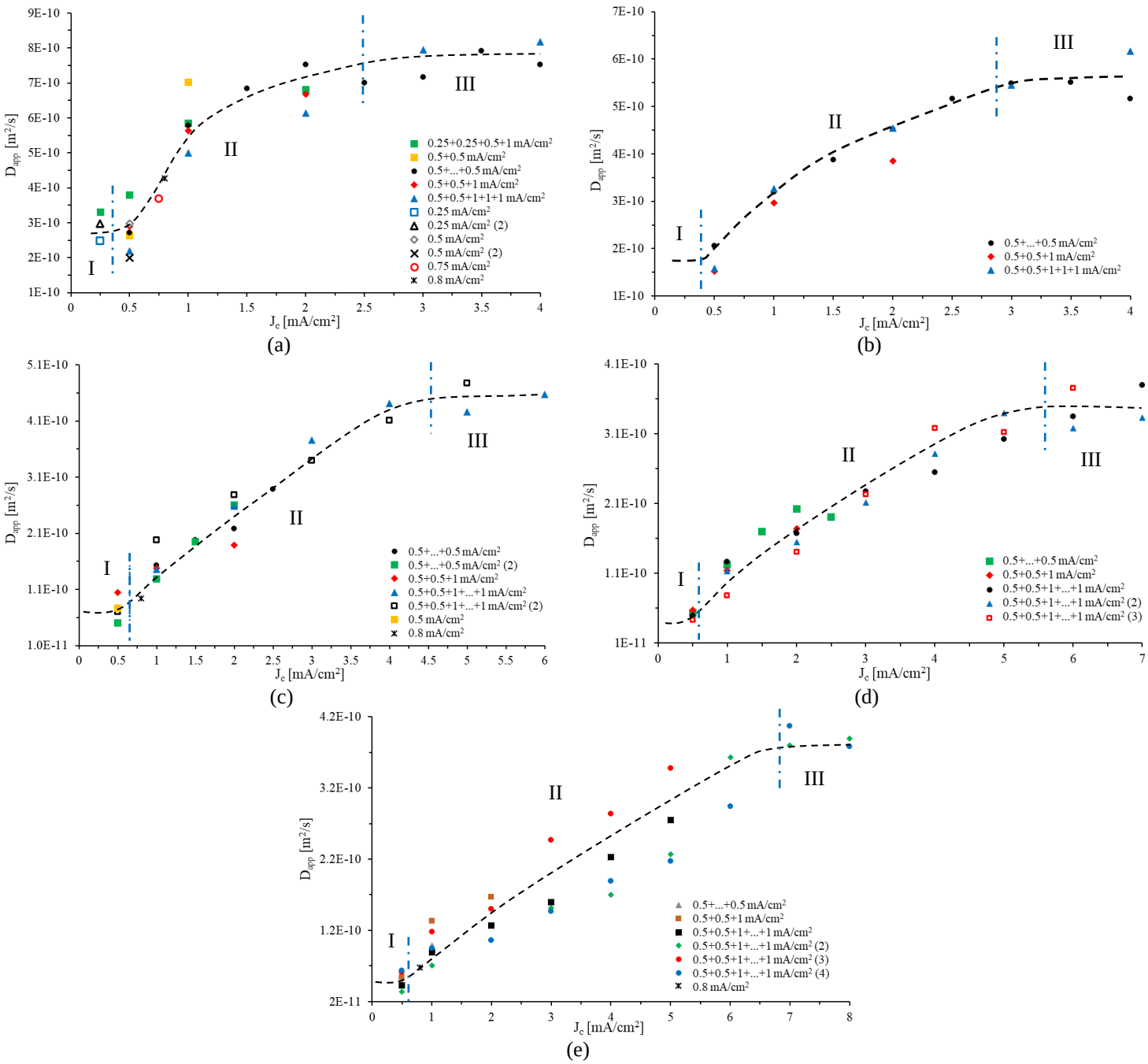

Figure 12. Evolution of the apparent hydrogen diffusion coefficient, D_{app}, with the applied cathodic current density, J_c, obtained in all the build-up permeation tests performed on the 42CrMo4 steel grade quenched and tempered at (a) 700, (b) 650, (c) 600, (d) 550 and (e) 500ºC

In agreement with the theoretical work developed by Raina et al. [83], which was also experimentally demonstrated in a previous paper regarding the 42CrMo4 steel quenched and tempered at 700ºC [53], three different hydrogen diffusion regimes may be distinguished in all these transient permeation tests, depending on trap occupancy:

(I) At the beginning of the tests, the hydrogen traps are completely empty. Hence, in the first build-up transient (always under a J_c value of 0.5 mA/cm² in our experiments), the apparent diffusion coefficient is the lowest, as the interaction of hydrogen atoms with microstructural traps is maximal.

(II) During the following build-up transients, hydrogen atoms progressively fill the microstructural traps present in the steel microstructure. Trapping effects gradually decrease and, hence, the value of D_{app} increases continuously throughout this regime.

(III) Finally, the hydrogen diffusion coefficient becomes practically constant, regardless of the applied cathodic current density, which means that the hydrogen traps have become saturated and there are no more trapping effects, only lattice diffusion. Consequently, this value corresponds to the so-called lattice hydrogen diffusion coefficient of the steel, D_L.

3.3.1. Trapping density

Table 8 presents the density of trapping sites, N_t, determined in all the studied steel grades considering low trap occupancy, Equation (3), and high trap occupancy, Equation (5). Dislocations were assumed to be the governing trapping sites in quenched and tempered martensitic steels (hydrogen traps with the highest binding energy). Thus, a trap binding energy of E_b=27 kJ/mol, determined in our TDA analysis (see Table 6), was applied to calculate N_t by means of Equation (4). Table 8 also contains the average values (considering all the tests performed for each steel grade) of the apparent sub-surface cathodic hydrogen concentration, C_{0app}, calculated when traps were saturated.

In line with the evolution of C_{0app}, a gradual increase in the density of trapping sites is observed when the tempering temperature decreased from 700ºC to 500ºC. Moreover, the density of trapping sites obtained using both equations were quite similar in all these steel grades. The last column in Table 8 shows the average value obtained using the results calculated with both equations.

Steel grade	HB	Low trap occupancy Equation (3)		High trap occupancy Equation (5),		Trap density (average)
		E_b [kJ/mol]	N_t [sites/m^3]	C_{0app} [ppm]	N_t [sites/m^3]	N_t [sites/m^3]
42CrMo4-700	201	27	$1.53\square10^{25}$	2.2	$1.49\square10^{25}$	$1.51\square10^{25}$
42CrMo4-650	246		$2.10\square10^{25}$	3.5	$3.33\square10^{25}$	$2.72\square10^{25}$
42CrMo4-600	281		$4.63\square10^{25}$	4.4	$5.30\square10^{25}$	$4.97\square10^{25}$
42CrMo4-550	307		$5.68\square10^{25}$	5.0	$7.78\square10^{25}$	$6.73\square10^{25}$
42CrMo4-500	335		$7.25\square10^{25}$	5.9	$8.33\square10^{25}$	$7.79\square10^{25}$

Table 8. Apparent cathodic hydrogen concentration, C_{oapp}, and density of trapping sites N_t calculated for all the steel grades

4. DISCUSSION

Figure 13 represents the average values of D_{app} showed in Figure 12 on a plot of D_{app} vs. J_c. The apparent diffusion coefficient increases with increasing applied cathodic current density and, at the same time, can also be seen to increase for any current density when the steel is tempered at a higher temperature.

Additionally, in order to provide a quantitative visualization of the results, Table 9 presents the average values of the apparent hydrogen diffusion coefficient, D_{app}, determined using a very low cathodic current density (0.5 mA/cm^2), when most traps are empty, and that of the lattice hydrogen diffusion coefficient, D_L, once trap saturation is reached under a certain cathodic current density level. The J_c values needed for hydrogen saturation are also included in this table.

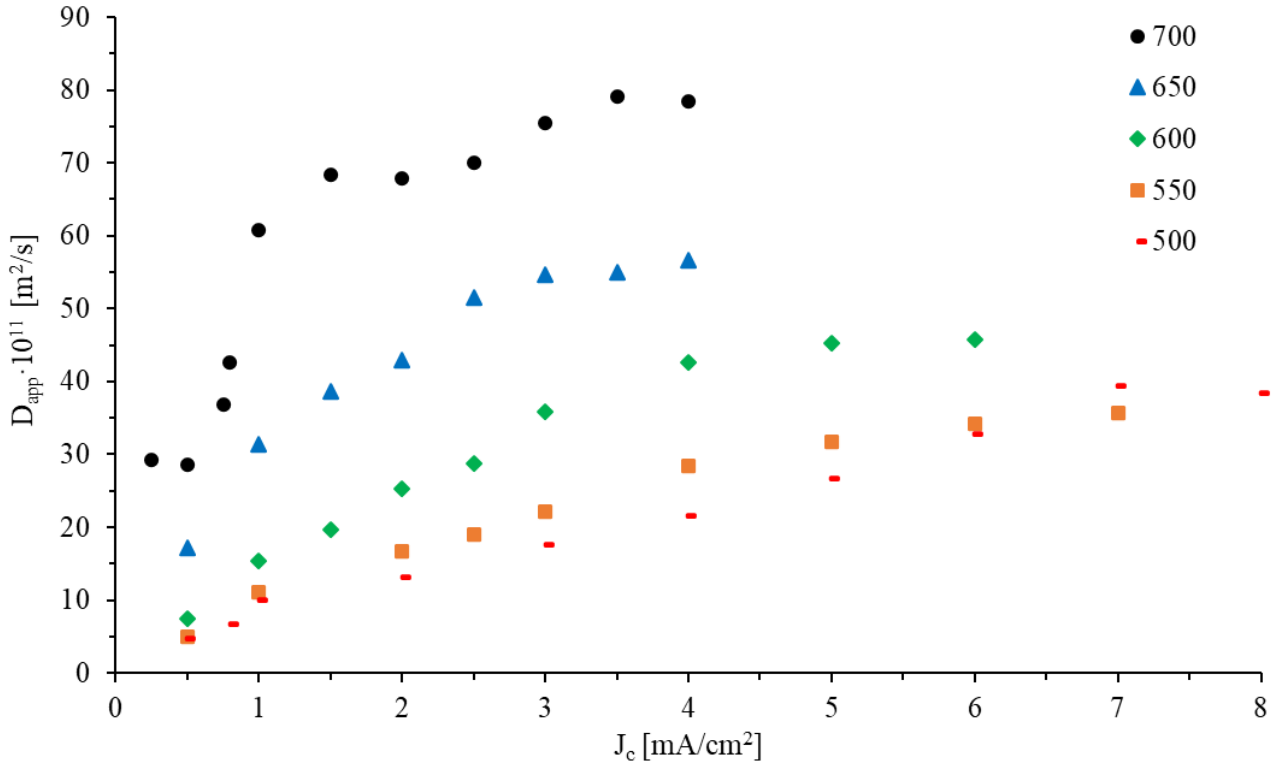

Figure 13. Representation of D_{app} vs. J_c for all the studied 42CrMo4 steel grades (average values taken from Figure 12)

Steel Grade	HB	FWHM [º]	D_{app} [m²/s]	D_L [m²/s]	J_c saturation [mA/cm²]
42CrMo4-700	201	1.79	$2.9 \cdot 10^{-10}$	$7.6 \cdot 10^{-10}$	2-3
42CrMo4-650	246	1.93	$1.7 \cdot 10^{-10}$	$5.5 \cdot 10^{-10}$	3-3.5
42CrMo4-600	281	2.00	$7.5 \cdot 10^{-11}$	$4.5 \cdot 10^{-10}$	4-5
42CrMo4-550	307	2.23	$5.0 \cdot 10^{-11}$	$3.5 \cdot 10^{-10}$	5.5-6
42CrMo4-500	335	2.41	$4.4 \cdot 10^{-11}$	$3.8 \cdot 10^{-10}$	6.5-7

Table 9. Average apparent (D_{app}) and lattice (D_L) hydrogen diffusion coefficients and cathodic current density (J_c) for saturation of each 42CrMo4 steel grade

It can be seen that both diffusion parameters, D_{app} and D_L, decrease with decreasing tempering temperature. In fact, the D_{app} and D_L values of the steel grade tempered at 700ºC are respectively around 7 and 2 times greater than those of the steel tempered at 500ºC. Furthermore, the harder steel grades need a significantly higher cathodic current density to reach saturation, i.e. more hydrogen may be generated on the cathodic side of the specimen to fill all its microstructural traps.

Fig. 14 shows the relationship between the steel hardness, HB, the value of the apparent hydrogen diffusion coefficient, D_{app}, for low trap occupancy (first permeation transient using 0.5 mA/cm², in which most traps are empty), the lattice hydrogen diffusion coefficient, D_L, when the microstructural traps were saturated with hydrogen (last permeation transient) and the value of the apparent sub-surface hydrogen concentration on the charging side of the specimen, C_{0app}, when the specimen has reached saturation (J_c saturation). Note the excellent correlation between the aforementioned permeation properties and the hardness of the different steel grades. Hydrogen diffusivity decreases and hydrogen solubility increases continuously with steel hardness, which is in line with the results reported previously by other authors [20,72]. This behaviour can be attributed to the higher density of lattice imperfections, mainly dislocations, associated with hardness in quenched and tempered steels, which constitute the most significant structural parameter governing hydrogen diffusion and trapping in these steels.

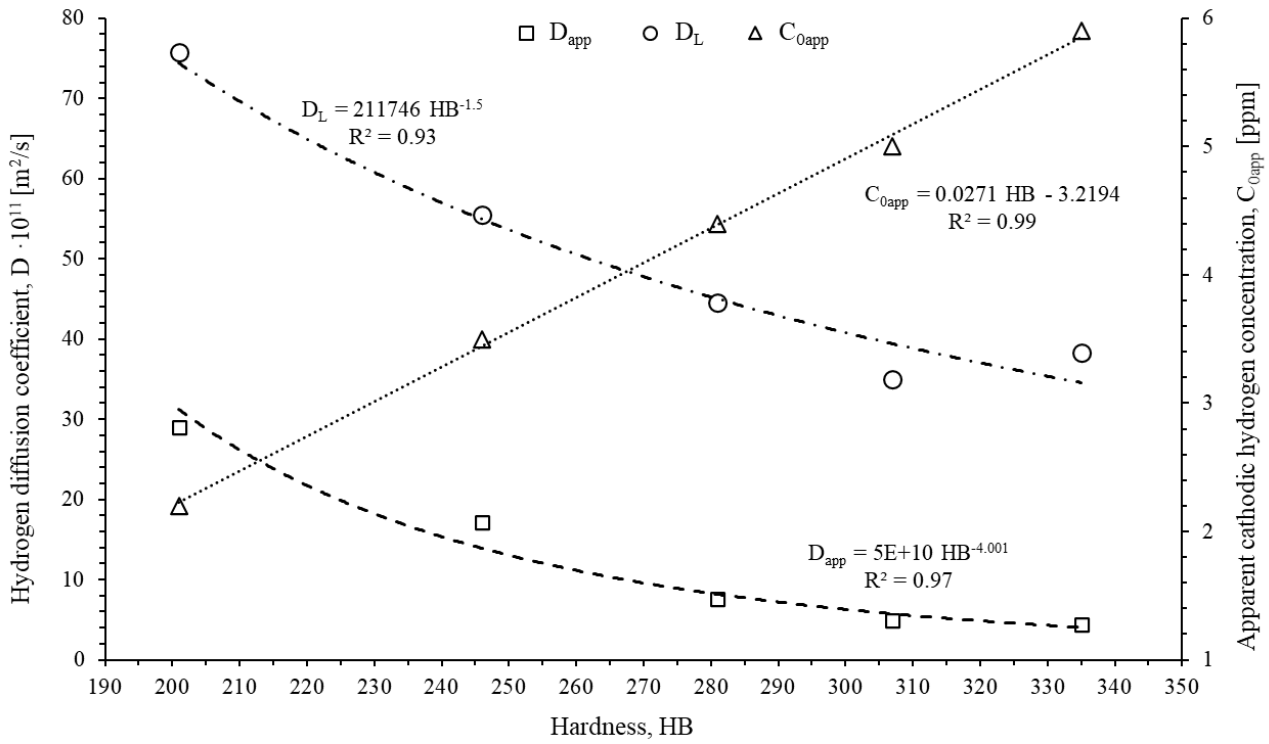

Figure 14. Relationship between HB hardness, lattice and apparent hydrogen diffusion coefficients, D_L and D_{app} and apparent sub-surface hydrogen concentration, C_{oapp}, for all the 42CrMo4 steel grades

Finally, Figure 15 shows the relationship between the Brinell hardness, HB, and the density of hydrogen trapping sites, N_t. Both Equation (6), for high trap occupancy, and Equation (4), for low trap occupancy, show that N_t values increase with increasing hardness, following potential laws with excellent fittings (R^2 determination coefficients of 0.98 and 0.95 were obtained respectively). The average trap density, N_t, obtained using the results calculated by means of both equations shows an even better potential fitting (R^2=0.99).

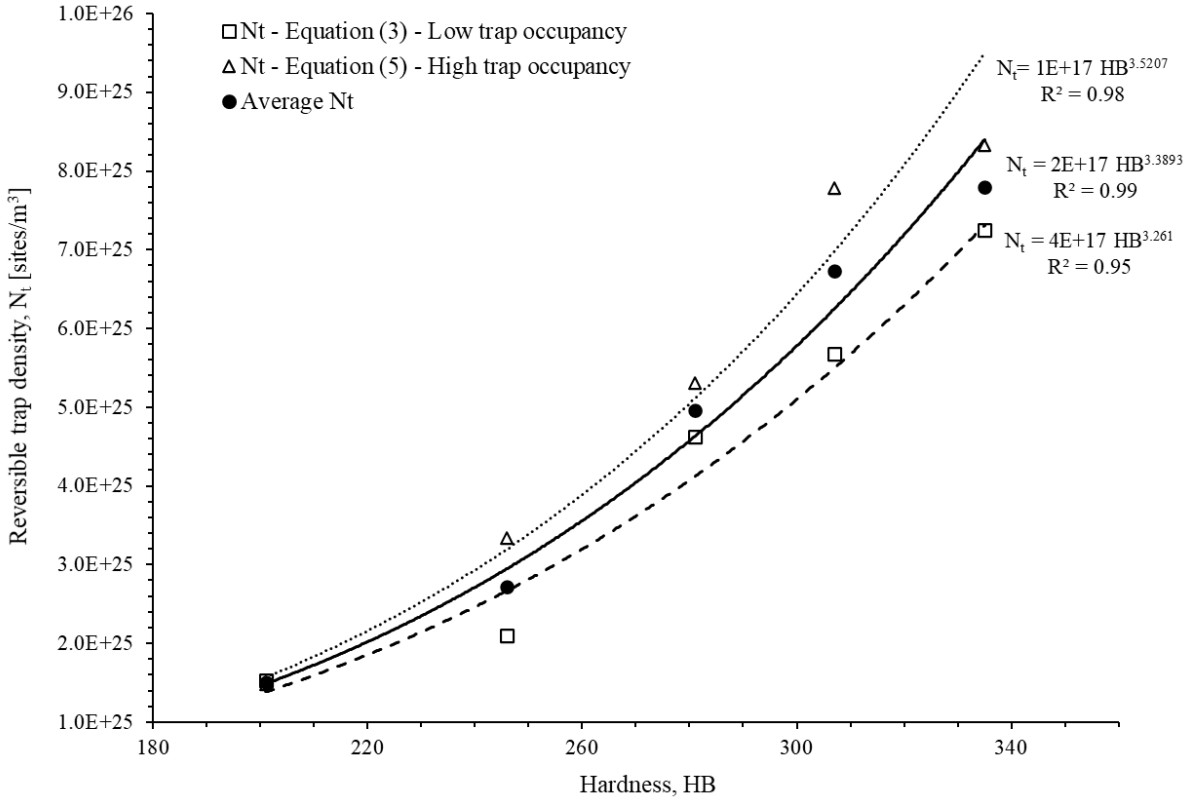

Fig. 15. Relationship between HB hardness and hydrogen trap density sites, Nt. Low trap occupancy (Equation 4, E_b=27 kJ/mol), high trap occupancy (Equation 6) and average trap density, N_t.

5. CONCLUSIONS

Hydrogen binding energies of 11.8, 17 and 27.4 kJ/mol were determined by applying thermal desorption analysis to a quenched and tempered 42CrMo4 steel, these values were found not to depend on the tempering temperature (between 500 and 700ºC). It was demonstrated that the peak with the highest energy (with a hydrogen binding energy of 27.4 kJ/mol) is associated with dislocations, the magnitude of this peak being inversely proportional to the tempering temperature (given that the dislocation density decreases with increasing tempering temperature).

Moreover, by means of stepped build-up permeation transients, three hydrogen diffusion regimes were defined depending on trap occupancy. In the first transient, when the hydrogen traps are empty, the lowest apparent diffusion coefficient, D_{app}, is measured, as the interaction of hydrogen atoms with microstructural traps is maximal (Regime I). During the following build-up transients, hydrogen atoms progressively fill the microstructural traps present in the steel microstructure and D_{app} increases continuously (Regime II), until D_{app} becomes practically constant, when all the hydrogen traps become saturated and this value is the lattice hydrogen diffusion coefficient, D_L (Regime III).

Both hydrogen diffusivities, D_{app} and D_L, decrease and hydrogen solubility, C_{0app}, (subsurface hydrogen concentration at the entry side when all the traps are filled) and the density of hydrogen traps, N_t, increase with steel hardness. Hardness varies linearly with the tempering temperature in this 42CrMo4 quenched steel, as all these parameters are known to be highly dependent on the density of dislocations, which is in turn known to constitute the most important hydrogen trapping sites present in the microstructure of quenched and tempered alloyed steels. The D_{app} and D_L values of the steel grade tempered at 700ºC are respectively around 7 and 2 times greater than those of the steel tempered at 500ºC. Furthermore, the harder

steel grades need a significantly higher cathodic current density to reach trap saturation, i.e. more hydrogen may be generated on the cathodic side of the specimen to fill all its microstructural traps.

AKNOWLEDGEMENTS

The authors would like to thank the Spanish Ministry of Science, Innovation and Universities for the financial support received to carry out research project RTI2018-096070-B-C31 (H2steelweld). Moreover, A. Zafra is likewise grateful to the Ministry of Education and Culture of the Principality of Asturias for his Severo Ochoa grant (PA-18-PF-BP17-038). Authors also thank the financial support received from the Principado de Asturias government through the FC-GRUPIN-IDI/2018/000134 project.

REFERENCES

[1] C.D. Kim, Hydrogen-damage failures, in: Met. Handbook, Vol.11, Fail. Anal. Prev., American Society for Metals, Metals Park, Ohio, Estados Unidos, 1986.

[2] A.L. Marcelo, R.C. Tokimatsu, I. Ferreira, Hydrogen embrittlement in an AISI 1045 steel component of the sugarcane industry, Eng. Fail. Anal. 16 (2009) 468–474.

[3] G. Straffelini, L. Versari, Brittle intergranular fracture of a thread: The role of a carburizing treatment, Eng. Fail. Anal. 16 (2009) 1448–1453.

[4] M. Yan, Y. Weng, Study on hydrogen absorption of pipeline steel under cathodic charging, Corros. Sci. 48 (2006) 432–444.

[5] S. Takagi, Y. Toji, M. Yoshino, K. Hasegawa, Hydrogen embrittlement resistance evaluation of ultra high strength steel sheets for automobiles, ISIJ Int. 52 (2012) 316–322.

[6] A. Oudriss, A. Fleurentin, G. Courlit, E. Conforto, C. Berziou, C. Rébéré, S. Cohendoz, J.M. Sobrino, J. Creus, X. Feaugas, Consequence of the diffusive hydrogen contents on tensile properties of martensitic steel during the desorption at room temperature, Mater. Sci. Eng. A. 598 (2014) 420–428.

[7] Y. Murakami, T. Kanezaki, P. Sofronis, Hydrogen embrittlement of high strength steels: Determination of the threshold stress intensity for small cracks nucleating at nonmetallic inclusions, Eng. Fract. Mech. 97 (2012) 227–243.

[8] C. Colombo, G. Fumagalli, F. Bolzoni, G. Gobbi, L. Vergani, Fatigue behavior of hydrogen pre-charged low alloy Cr-Mo steel, Int. J. Fatigue. 83 (2015) 2–9.

[9] E. Ohaeri, U. Eduok, J. Szpunar, Hydrogen related degradation in pipeline steel: A review, Int. J. Hydrogen Energy. 43 (2018) 14584–14617.

[10] H. Barthelemy, M. Weber, F. Barbier, Hydrogen storage: Recent improvements and industrial perspectives, Int. J. Hydrogen Energy. 42 (2017) 7254–7262.

[11] T. Zakroczymski, Adaptation of the electrochemical permeation technique for studying entry, transport and trapping of hydrogen in metals, Electrochim. Acta. 51 (2006) 2261–2266.

[12] S. Frappart, X. Feaugas, J. Creus, F. Thebault, L. Delattre, H. Marchebois, Study of the hydrogen diffusion and segregation into FeCMo martensitic HSLA steel using electrochemical permeation test, J. Phys. Chem. Solids. 71 (2010) 1467–1479.

[13] H. Husby, M. Iannuzzi, R. Johnsen, M. Kappes, A. Barnoush, Effect of nickel on hydrogen permeation in ferritic/pearlitic low alloy steels, Int. J. Hydrogen Energy. 43 (2018) 3845–3861.

[14] A. Turnbull, Perspectives on hydrogen uptake, diffusion and trapping, Int. J. Hydrogen Energy.

40 (2015) 16961–16970.

[15] Q. Liu, J. Venezuela, M. Zhang, Q. Zhou, A. Atrens, Hydrogen trapping in some advanced high strength steels, Corros. Sci. 111 (2016) 770–785.

[16] A. Turnbull, R.B. Hutchings, D.H. Ferriss, Modelling of thermal desorption of hydrogen from metals, Mater. Sci. Eng. A. 238 (1997) 317–328.

[17] J. Takahashi, K. Kawakami, Y. Kobayashi, Origin of hydrogen trapping site in vanadium carbide precipitation strengthening steel, Acta Materialia Inc., 2018.

[18] E. Legrand, A. Oudriss, C. Savall, J. Bouhattate, X. Feaugas, Towards a better understanding of hydrogen measurements obtained by thermal desorption spectroscopy using FEM modeling, Int. J. Hydrogen Energy. 40 (2015) 2871–2881.

[19] N. Ishikawa, H. Sueyoshi, A. Nagao, Hydrogen microprint analysis on the effect of dislocations on grain boundary hydrogen distribution in steels, ISIJ Int. 56 (2016) 413–417.

[20] F.G. Wei, K. Tsuzaki, Hydrogen trapping phenomena in martensitic steels, Gaseous Hydrog. Embrittlement Mater. Energy Technol. Probl. Its Characterisation Eff. Part. Alloy Classes. (2012) 493–525.

[21] D.C.S. Garcia, R.N. Carvalho, V.F.C. Lins, D.M. Rezende, D.S. Dos Santos, Influence of microstructure in the hydrogen permeation in martensitic-ferritic stainless steel, Int. J. Hydrogen Energy. 40 (2015) 17102–17109.

[22] R.A. Oriani, The diffusion and trapping of hydrogen in steel, Acta Metall. 18 (1970) 147–157.

[23] K. Kiuchi, R.B. McLellan, The solubility and diffusivity of hydrogen in well-annealed and deformed iron, Acta Metall. 31 (1983) 961–984.

[24] L. Scoppio, M. Barteri, Methods of hydrogen uptake measurements by electrochemical permeation tests on low alloy steels, in: A. Turnbull (Ed.), Hydrogen transport and cracking in metals. Proceedings of a conference, Teddington UK, 1995: pp. 204–215.

[25] L. Moli-Sanchez, F. Martin, E. Leunis, J. Chene, M. Wery, Hydrogen transport in 34CrMo4 martensitic steel: Influence of microstructural defects on H diffusion, Defect Diffus. Forum. 323–325 (2012) 485–490.

[26] T. Zakroczymski, Electrochemical determination of hydrogen in metals, J. Electroanal. Chem. 475 (1999) 82–88.

[27] J.O. Bockris, J. McBreen, L. Nanis, The Hydrogen Evolution Kinetics and Hydrogen Entry into a-Iron, J. Electrochem. Soc. 112 (1965) 1025–1031.

[28] N. Parvathavarthini, S. Saroja, R.K. Dayal, H.S. Khatak, Studies on hydrogen permeability of 2.25% Cr-1% Mo ferritic steel: Correlation with microstructure, J. Nucl. Mater. 288 (2001) 187–196.

[29] M. Garet, A.M. Brass, C. Haut, F. Guttierez-Solana, Hydrogen trapping on non metallic inclusions in Cr-Mo low alloy steels, Corros. Sci. 40 (1998) 1073–1086.

[30] T. Depover, K. Verbeken, Thermal desorption spectroscopy study of the hydrogen trapping ability of W based precipitates in a Q&T matrix, Int. J. Hydrogen Energy. 43 (2018) 5760–5769.

[31] E.I. Galindo-Nava, B.I.Y. Basha, P.E.J. Rivera-Díaz-del-Castillo, Hydrogen transport in metals: Integration of permeation, thermal desorption and degassing, J. Mater. Sci. Technol. 33 (2017) 1433–1447.

[32] A. Zafra, L.B. Peral, J. Belzunce, C. Rodríguez, Effect of hydrogen on the tensile properties of 42CrMo4 steel quenched and tempered at different temperatures, Int. J. Hydrogen Energy. 43 (2018) 9068–9082.

[33] A. Zafra, L.B. Peral, J. Belzunce, C. Rodríguez, Effects of hydrogen on the fracture toughness of 42CrMo4 steel quenched and tempered at different temperatures, Int. J. Press. Vessel. Pip. 171 (2019) 34–50.

[34] G.K. Williamson, R.E. Smallman, III. Dislocation densities in some annealed and cold-worked metals from measurements on the X-ray Debye-Scherrer spectrum, Philos. Mag. 1 (1956) 34–46.

[35] M.N. Yoozbashi, S. Yazdani, XRD and TEM study of bainitic ferrite plate thickness in nanostructured, carbide free bainitic steels, Mater. Chem. Phys. 160 (2015) 148–154.

[36] S. Takebayashl, T. Kunieda, N. Yoshinaga, K. Ushioda, S. Ogata, Comparison of the dislocation density in martensitic steels evaluated by some X-ray diffraction methods, ISIJ Int. 50 (2010) 875–882.

[37] A. Nagao, M. Dadfarnia, B.P. Somerday, P. Sofronis, R.O. Ritchie, Hydrogen-enhanced-plasticity mediated decohesion for hydrogen-induced intergranular and "quasi-cleavage" fracture of lath martensitic steels, J. Mech. Phys. Solids. 112 (2018) 403–430.

[38] M. Nagumo, Fundamentals of hydrogen embrittlement, 2016.

[39] T. Schaffner, A. Hartmaier, V. Kokotin, M. Pohl, Analysis of hydrogen diffusion and trapping in ultra-high strength steel grades, J. Alloys Compd. 746 (2018) 557–566.

[40] W.Y. Choo, J.Y. Lee, Thermal Analysis of Trapped Hydrogen in Pure Iron, 13 (1982) 423–427.

[41] J.Y. Lee, J.L. Lee, J.L. Lee, A trapping theory of hydrogen in pure iron, Philos. Mag. A Phys. Condens. Matter, Struct. Defects Mech. Prop. 56 (1987) 293–309.

[42] A. López-Suárez, Influence of surface roughness on consecutively hydrogen absorption cycles in Ti-6Al-4V alloy, Int. J. Hydrogen Energy. 35 (2010) 10404–10411.

[43] J.A. Carreño, I. Uribe, J.C. Carrillo, Modelling of roughness effect on hydrogen permeation in a low carbon steel, Rev. Metal. (2003) 213–218.

[44] R. Réquiz, N. Vera, S. Camero, The influence of surface roughness on the hydrogen permeation of type API 5L-X52 steel, Rev. Metal. 40 (2004) 30–38.

[45] M.A. V Devanathan, Z. Stachurski, The adsorption and diffusion of electrolytic hydrogen in palladium, Proc. R. Soc. London. Ser. A. Math. Phys. Sci. 270 (1962) 90–102.

[46] ASTM G148, Standard practice for evaluation of hydrogen uptake, permeation, and transport in metals by an electrochemical technique, ASTM Int. (2011).

[47] T. Zakroczymski, Z. Szklarska- Śmiałowska, M. Smialowski, Effect of Arsenic on Permeation of Hydrogen Through Steel Membranes polarized cathodically in aqueous solution, Mater. Corros. 26 (1975) 617–624.

[48] R. Valentini, A. Salina, Influence of microstructure on hydrogen embrittlement behaviour of 2·25Cr–1 Mo steel, Mater. Sci. Technol. (United Kingdom). 10 (1994) 908–914.

[49] S. Ningshen, M. Uhlemann, F. Schneider, H.S. Khatak, Diffusion behaviour of hydrogen in nitrogen containing austenitic alloys, Corros. Sci. 43 (2001) 2255–2264.

[50] P. Manolatos, M. Jerome, J. Galland, Necessity of a palladium coating to ensure hydrogen oxidation during electrochemical permeation measurements on iron, Electrochim. Acta. 40 (1995) 867–871.

[51] E. Fallahmohammadi, F. Bolzoni, L. Lazzari, Measurement of lattice and apparent diffusion coefficient of hydrogen in X65 and F22 pipeline steels, Int. J. Hydrogen Energy. 38 (2013) 2531–2543.

[52] D. Rudomilova, T. Prošek, P. Salvetr, A. Knaislová, P. Novák, R. Kodým, G. Schimo-Aichhorn, A. Muhr, H. Duchaczek, G. Luckeneder, The effect of microstructure on hydrogen permeability

of high strength steels, Mater. Corros. (2019).

[53] A. Zafra, J. Belzunce, C. Rodríguez, Hydrogen diffusion and trapping in 42CrMo4 quenched and tempered steel: influence of quenching temperature and plastic deformation, Under Rev. (2020).

[54] J. Kittel, X. Feaugas, J. Creus, Impact of charging conditions and membrane thickness on hydrogen permeation through steel: Thick/thin membrane concepts revisited, NACE - Int. Corros. Conf. Ser. 2 (2016) 858–878.

[55] J. Kittel, F. Ropital, J. Pellier, New insights into hydrogen permeation in steels: Measurements through thick membranes, NACE - Int. Corros. Conf. Ser. (2008) 084091–0840922.

[56] A. McNabb & P.K. Foster, A new analysis of the diffusion of hydrogen in iron and ferritic steels, Trans. Met. Soc. AIME. 227 (1963) 618–27.

[57] A.J. Kumnick, H.H. Johnson, Hydrogen Transport Through Annealed and Deformed Armco Iron., Met. Trans. 5 (1974) 1199–1206.

[58] A.J. Kumnick, H.H. Johnson, Deep Trapping for Hydrogen Iron, Acta Metall. 28 (1980) 33–39.

[59] A.H.M. Krom, A.D. Bakker, Hydrogen trapping models in steel, Metall. Mater. Trans. B Process Metall. Mater. Process. Sci. 31 (2000) 1475–1482.

[60] S.K. Yen, I.B. Huang, Critical hydrogen concentration for hydrogen-induced blistering on AISI 430 stainless steel, Mater. Chem. Phys. 80 (2003) 662–666.

[61] C.F. Dong, Z.Y. Liu, X.G. Li, Y.F. Cheng, Effects of hydrogen-charging on the susceptibility of X100 pipeline steel to hydrogen-induced cracking, Int. J. Hydrogen Energy. 34 (2009) 9879–9884.

[62] H. Izadi, M. Tavakoli, M.H. Moayed, Effect of thermomechanical processing on hydrogen permeation in API X70 pipeline steel, Mater. Chem. Phys. 220 (2018) 360–365.

[63] R.A. Renzetti, H.R.Z. Sandim, R.E. Bolmaro, P.A. Suzuki, A. Möslang, X-ray evaluation of dislocation density in ODS-Eurofer steel, Mater. Sci. Eng. A. 534 (2012) 142–146.

[64] P. Castaño-Rivera, N.S. De Vincentis, R.E. Bolmaro, P. Bruzzoni, Relationship between Dislocation Densityand Hydrogen Trappingin a Cold Worked API 5L X60 Steel, Procedia Mater. Sci. 8 (2015) 1031–1038.

[65] J. Pešička, R. Kužel, A. Dronhofer, G. Eggeler, The evolution of dislocation density during heat treatment and creep of tempered martensite ferritic steels, Acta Mater. 51 (2003) 4847–4862.

[66] F.G. Wei, K. Tsuzaki, Response of hydrogen trapping capability to microstructural change in tempered Fe-0.2C martensite, Scr. Mater. 52 (2005) 467–472.

[67] W. Krieger, S. V Merzlikin, A. Bashir, A. Szczepaniak, Spatially resolved detection with Scanning Kelvin Probe Force Microscopy (SKPFM), Acta Mater. (2017).

[68] M. Dadfarnia, P. Sofronis, T. Neeraj, Hydrogen interaction with multiple traps: Can it be used to mitigate embrittlement?, Int. J. Hydrogen Energy. 36 (2011) 10141–10148.

[69] D. Li, R.P. Gangloff, J.R. Scully, Hydrogen Trap States in Ultrahigh-Strength AERMET 100 Steel, Metall. Mater. Trans. A Phys. Metall. Mater. Sci. 35 A (2004) 849–864.

[70] W.Y. Choo, J.Y. Lee, Effect of cold working on the hydrogen trapping phenomena in pure iron, Metall. Trans. A. 14 (1983) 1299–1305.

[71] J.S. Kim, Y.H. Lee, D.L. Lee, K.T. Park, C.S. Lee, Microstructural influences on hydrogen delayed fracture of high strength steels, Mater. Sci. Eng. A. 505 (2009) 105–110.

[72] Y. Sakamoto, T. Mantani, Effect of quenching and tempering on diffusion of hydrogen in carbon steel, Trans. JIM. 17 (1976).

[73] P. Zhou, W. Li, H. Zhao, X. Jin, Role of microstructure on electrochemical hydrogen permeation properties in advanced high strength steels, Int. J. Hydrogen Energy. 43 (2018) 10905–10914.

[74] A.J. Haq, K. Muzaka, D.P. Dunne, A. Calka, E. V. Pereloma, Effect of microstructure and composition on hydrogen permeation in X70 pipeline steels, Int. J. Hydrogen Energy. 38 (2013) 2544–2556.

[75] H.K.D.H. Bhadeshia, Prevention of hydrogen embrittlement in steels, ISIJ Int. 56 (2016) 24–36.

[76] R. Gibala and A.J. Kumnick, Hydrogen Trapping in Iron and Steels, in: R. Gibala and R.F. Hehemann (Ed.), Hydrog. Embrittlement Stress Corros. Crack., American Society for Metals, Metals Park, Ohio, USA, 1984: pp. 61–77.

[77] A.B. Hadžipašić, J. Malina, Š. Nižník, The influence of microstructure on hydrogen diffusion in dual phase steel, Acta Metall. Slovaca. 17 (2011) 129–137.

[78] M. Enomoto, D. Hirakami, T. Tarui, Modeling thermal desorption analysis of hydrogen in steel, ISIJ Int. 46 (2006) 1381–1387.

[79] H. Hagi, Effect of interface between cementite and ferrite on diffusion of hydrogen in carbon steels, Mater. Trans. JIM. 35 (1994) 168–173.

[80] I. Maroef, D.L. Olson, M. Eberhart, G.R. Edwards, Hydrogen trapping in ferritic steel weld metal, Int. Mater. Rev. 47 (2002) 191–223.

[81] B.J. Berkowitz, F.H. Heubaum, Dislocation Transport of Hydrogen in Steel., NATO Conf. Ser. 6 Mater. Sci. 5 (1983) 823–827.

[82] M. Kurkela, G.S. Frankel, R.M. Latanision, S. Suresh, R.O. Ritchie, Influence of plastic deformation on hydrogen transport in 2 1 4 Cr-1Mo steel, Scr. Metall. 16 (1982) 455–459.

[83] A. Raina, V.S. Deshpande, N.A. Fleck, Analysis of thermal desorption of hydrogen in metallic alloys, Acta Mater. 144 (2018) 777–785.